NASA TECHNICAL MEMORANDUM

NASA TM X-53423

March 30, 1966

NASA TM X-53423

STATIC AERODYNAMIC CHARACTERISTICS OF THE ABORTED APOLLO-SATURN IB VEHICLE

By Billy W. Nunley
Aero-Astrodynamics Laboratory

NASA

George C. Marshall Space Flight Center, Huntsville, Alabama

TECHNICAL MEMORANDUM X-53423

STATIC AERODYNAMIC CHARACTERISTICS OF THE ABORTED APOLLO-SATURN IB VEHICLE

By

Billy W. Nunley

ABSTRACT

23586

Aerodynamic characteristics of the aborted Apollo-Saturn IB vehicles are defined for control and structural analyses. Static stability characteristics are presented at various angles of attack (0° - 15°) as a function of Mach number. Local normal force coefficient distributions are included at various angles of attack (0° - 15°) for the Mach numbers ranging from 0.5 to 2.86. Axial force coefficients for power-off and power-on conditions are defined at zero angle of attack throughout the Mach number range. Local axial force coefficient and local pressure coefficient distributions are presented at zero angle of attack at Mach numbers from 0.5 to 2.86. These data are based primarily on wind tunnel tests of scale models.

Author

NASA-GEORGE C. MARSHALL SPACE FLIGHT CENTER

NASA-GEORGE C. MARSHALL SPACE FLIGHT CENTER

TECHNICAL MEMORANDUM X-53423

March 30, 1966

STATIC AERODYNAMIC CHARACTERISTICS OF THE ABORTED APOLLO-SATURN IB VEHICLE

By

Billy W. Nunley

VEHICLE AERODYNAMICS SECTION
AERODYNAMIC DESIGN BRANCH
AERODYNAMICS DIVISION
AERO-ASTRODYNAMICS LABORATORY

LIST OF ILLUSTRATIONS

LIST OF ILLUSTRATIONS (Continued)

LIST OF ILLUSTRATIONS (Continued)

DEFINITION OF SYMBOLS

Symbol	Definition
A	Axial force
A_b	Base area
C_A	Axial force coefficient, A/qS
C'_A	Local axial force coefficient, $dC_A/d(X/D)$
C_{A_b}	S-IB/S-IVB interstage base axial force coefficient
$C_{A_{base}}$	Base axial force coefficient
C_{A_F}	Forebody axial force coefficient
$C_{A_{fins}}$	Fins axial force coefficient
$C_{A_{friction}}$	Friction axial force coefficient, per caliber
C_N	Normal force coefficient, N/qS
C'_N	Local normal force coefficient, $dC_N/d(X/D)$
C_{N_α}	Normal force coefficient gradient, $dC_N/d\alpha$
C'_{N_α}	Local normal force coefficient gradient, $dC_{N_\alpha}/d(X/D)$
$C_{N_{fins}}$	Fins normal force coefficient
$C_{N_{\alpha_{fins}}}$	Fins normal force coefficient gradient
CP/D	Center of pressure, calibers from station 100
$(CP/D)_{fins}$	Fin center of pressure, calibers from station 100

DEFINITION OF SYMBOLS

Symbol	Definition
C_p	Local pressure coefficient, $(P_L - P_\infty)/q$
$C_{p_{base}}$	Base pressure coefficient, $(P_B - P_\infty)/q$
$C_{p_{int}}$	Internal pressure coefficient, $(P_{int} - P_\infty)/q$
D_{ref}	Reference diameter, 257 inches
M_∞	Free stream Mach number
P_∞	Free stream static pressure
P_B	Base pressure
P_{int}	Internal pressure of spacecraft
P_L	Local pressure coefficient
q	Free stream dynamic pressure, $\frac{\gamma}{2} P_\infty M_\infty^2$
S	Reference area, $\pi D^2_{ref}/4$
X/D	Longitudinal distance from station 100, calibers
α	Angle of attack
γ	Ratio of specific heats

TECHNICAL MEMORANDUM X-53423

STATIC AERODYNAMIC CHARACTERISTICS OF THE ABORTED APOLLO-SATURN IB VEHICLE

SUMMARY

This report presents the static aerodynamic characteristics of the aborted Apollo-Saturn IB vehicle. These data are based primarily on wind tunnel tests of scale models. Static stability characteristics are included as a function of Mach number for angles of attack from 0° to 15°. Axial force characteristics are defined for power-on and power-off conditions at zero angle of attack as a function of Mach number. Local normal force coefficients are included at various angles of attack from 0° to 15° for Mach numbers from 0.5 to 2.86. Local pressure coefficient and axial force coefficient distributions are included for various Mach numbers from 0.5 to 2.86 at zero angle of attack.

I. INTRODUCTION

The primary mission of the research and development flights of the Apollo-Saturn IB vehicles is to demonstrate the compatibility and performance of the launch vehicle/spacecraft in preparation for manned flight. For the operational vehicles, the primary mission is to place a manned spacecraft in earth orbit. If a malfunction resulting in failure to complete the mission should occur during first stage flight, the command module will be aborted. If the malfunction occurs early in flight on unmanned vehicles, an attempt will be made to fly the aborted vehicle power-on until 60 seconds flight time has elapsed. On manned flights, this time has been decreased to 40 seconds. This requires a definition of the aerodynamic characteristics of the aborted Apollo-Saturn IB vehicle.

The aborted Apollo-Saturn IB vehicle consists of the S-IB first stage, S-IVB second stage, instrument unit (IU), lunar excursion module adapter (SLA), and service module (SM). The S-IB stage propulsive system includes eight Rocketdyne H-1 engines with a total sea level thrust of 1.6 million pounds. The S-IVB stage employs one Rocketdyne J-2 engine with a rated vacuum thrust of 200,000 pounds.

AS-201, AS-202, and AS-204 and subsequent are similar, the only major differences being in the base configuration. The S-IB stage of AS-201 is equipped with engine shrouds and side-mounted turbine exhaust ducts. For AS-202 and subsequent vehicles, the engine skirts will be

removed. AS-204 and subsequent vehicles will have the side-mounted turbine exhaust ducts removed, and the turbine exhaust gases will be vented through aspirators mounted on the inboard engine nozzles and directed into the flame shield area. The removals and installations discussed have significant effects only on the axial force characteristics; the proper accounting of these effects have been made for each vehicle.

A compatible difinition of the aerodynamic characteristics of the aborted Apollo-Saturn IB vehicles for trajectory, control, and structural analysis is presented. These data are based primarily on wind tunnel tests of scale models. Typical Apollo-Saturn IB trajectory data are presented in Figure 3. Data presented in this report will be applicable to all Apollo-Saturn IB vehicles provided there are no major configuration changes (such as frustum angles, stage lengths, etc.).

II. STATIC STABILITY CHARACTERISTICS

Static stability characteristics of the aborted Apollo-Saturn IB vehicle were defined based primarily on wind tunnel tests of scaled models. These tests were conducted at Chance Vought Corporation and Langley Research Center employing a 1.32 per cent scale model [3, 4]. Variations of center of pressure and normal force gradient at zero angle of attack are defined as a function of Mach number in Figure 4. The normal force coefficient as a function of angle of attack and Mach number is carpet-plotted in Figure 5. These data are presented for an angle of attack range of 0° to 15° and a Mach number range of 0 to 4.8. Corresponding center of pressure variations are presented in Figures 6 through 9. These data reflect the presence of protuberances and the effect on static stability characteristics.

III. AXIAL FORCE CHARACTERISTICS

Forebody axial force coefficient and power-off base axial force coefficient presented for each vehicle are based on wind tunnel tests of scaled models [3, 4]. Power-on base axial force coefficient was defined using flight data on Saturn I, Block II vehicles and wind tunnel tests of scaled models with simulated flow through the engines. By use of these data, total power-on and power-off axial force coefficients were defined at zero angle of attack as a function of Mach number.

Axial force characteristics of Apollo-Saturn 201, which reflect the presence of engine shrouds and externally mounted turbine exhaust ducts, are presented in Figure 10. Apollo-Saturn 202 axial force characteristics, presented in Figure 11, reflect the removal of engine shrouds and the presence of the turbine exhaust ducts. Axial force characteristics of

Apollo-Saturn 204 and subsequent vehicles, presented in Figure 12, reflect the removal of the engine shrouds and rerouting of the turbine exhaust gases into the flame shield area. Total power-on and power-off axial force, power-on and power-off base axial force, and forebody axial force coefficients are presented for each vehicle as a function of Mach number at zero angle of attack.

Variations of total power-on and power-off axial force during flight are defined as follows:

$$\text{Axial force (power-on)} = C_{A_T} \text{ (power-on) } q_\infty S$$

$$\text{Axial force (power-off)} = C_{A_T} \text{ (power-off) } q_\infty S$$

IV. LOCAL NORMAL FORCE COEFFICIENT DISTRIBUTIONS

Local normal force coefficient distributions, presented in Figures 13 through 36, are defined at Mach numbers from 0.5 to 2.86 for angle of attack from 2° to 15°. Fin contributions are included as concentrated loads on each figure at the proper longitudinal station. The fin normal force coefficient defines the forces of all eight fins and includes body upwash. The carry-over of the fins on the body is included in the load distributions over the body.

The local normal force coefficient distributions are based on wind tunnel tests of scale models [5 - 9]. Data from these tests were compiled to obtain a compatible definition of the load distribution over the vehicle. The contribution of the fins and tail barrel was obtained from Reference 6.

V. LOCAL AXIAL FORCE COEFFICIENT DISTRIBUTIONS

The distributions of local axial force coefficient, which are defined at zero angle of attack for various Mach numbers ranging from 0.5 to 2.86, were obtained from a scaled model pressure test [6]. The axial force coefficients of the flat face, S-IB/S-IVB base, shrouds, fins, power-on base, and power-off base are tabulated as concentrated loads since these data do not readily adapt to a distributed load. The tabulated fin and shroud loads were obtained from Reference 9 and the base axial force characteristics were obtained from Figures 10 through 12. The axial force coefficient for the flat face was obtained by assuming 90 per cent stagnation pressure over the face.

VI. LOCAL PRESSURE COEFFICIENT DISTRIBUTIONS

Longitudinal local pressure coefficient distributions were defined based on wind tunnel tests of scaled models. These data were obtained from the same sources as the local normal force coefficient distributions, [6 - 9], which are presented at zero angle of attack for Mach numbers ranging from 0.5 to 2.86 in Figures 40, 41, and 42.

When the command module is ejected, the spacecraft compartment is subjected to stagnation pressure. The internal pressure coefficient is defined as a function of Mach number in Figure 43.

CONCLUDING REMARKS

The data presented in this report are a compilation of aerodynamic characteristics necessary to support the design of the Apollo-Saturn IB launch vehicles. The purpose of this report is to supply an adequate and compatible definition of the aerodynamic characteristics for structural, control, and performance analysis.

The aerodynamic characteristics included are based primarily on wind tunnel tests of scaled models and supplemented with analytical data where experimental data were unavailable. The text of this report does not present a detailed analysis of the experimental data. This may be obtained from the referenced reports.

Blunt body aerodynamic data do not have the characteristic accuracy associated with that of complete launch vehicles. First, the increased bow shock strength and the greater potential for wind tunnel shock reflections reduce the probability of obtaining precise data. Furthermore, it has been shown for the extreme case of simple blunt cylinders that consistent data can be obtained in any single test series; yet it is difficult to obtain consistency between different test series. This is attributed to small discrepancies in shock fields, boundary layers, model geometries and scale, heat transfer effects, and flow field deviations. Nevertheless, the set of enclosed data is consistent and it is judged entirely adequate in terms of accuracy for conditions involved (i.e., a short term - unmanned flight before intentional destruction). If a judgement had to be made as to the probable accuracy, it would be as follows: normal force coefficient, $\pm$10 per cent; center of pressure, $\pm$0.4 caliber; and axial force coefficient, $\pm$15 per cent.

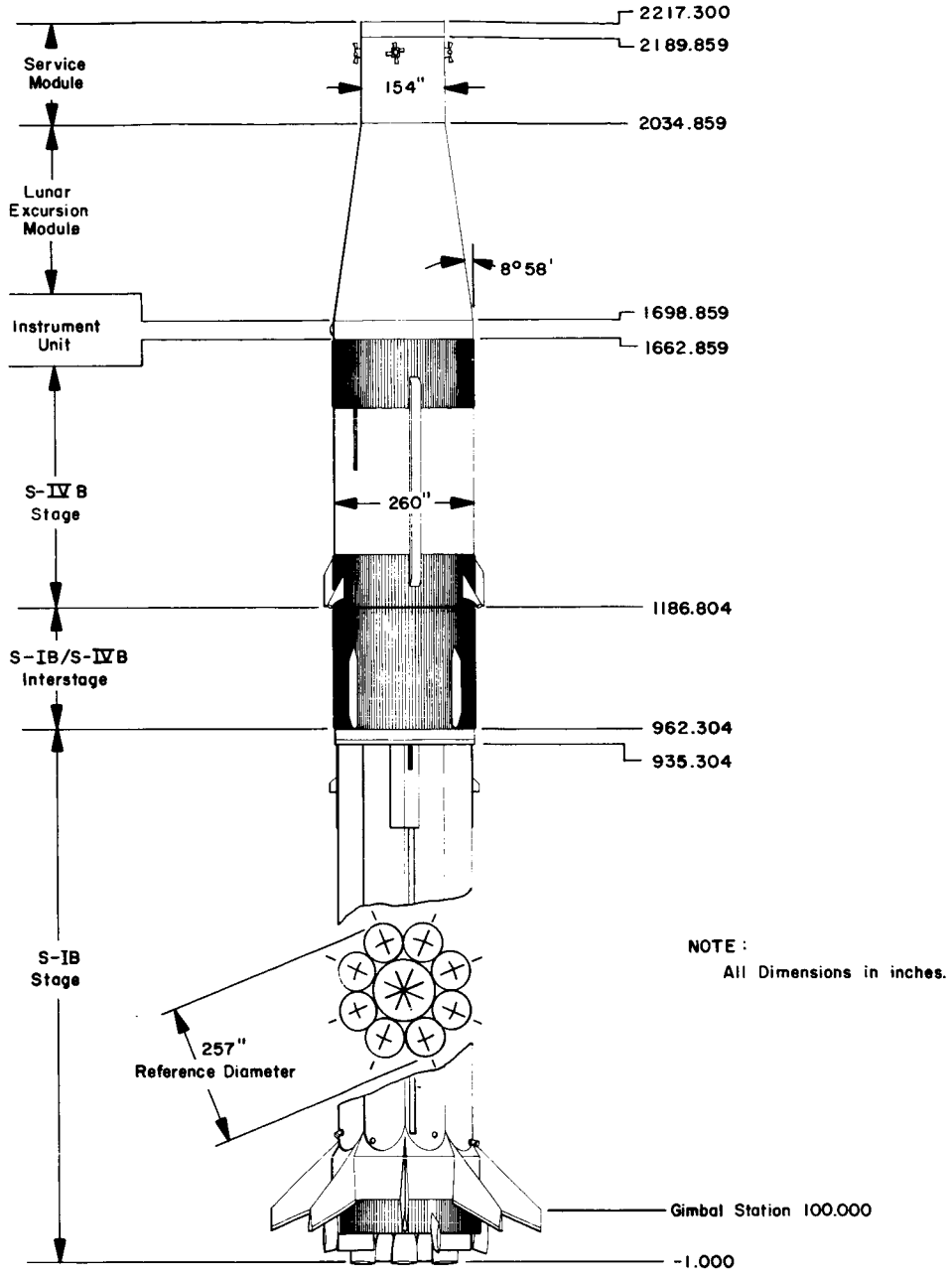

FIGURE 1 GEOMETRY OF THE ABORTED APOLLO-SATURN IB FLIGHT VEHICLE

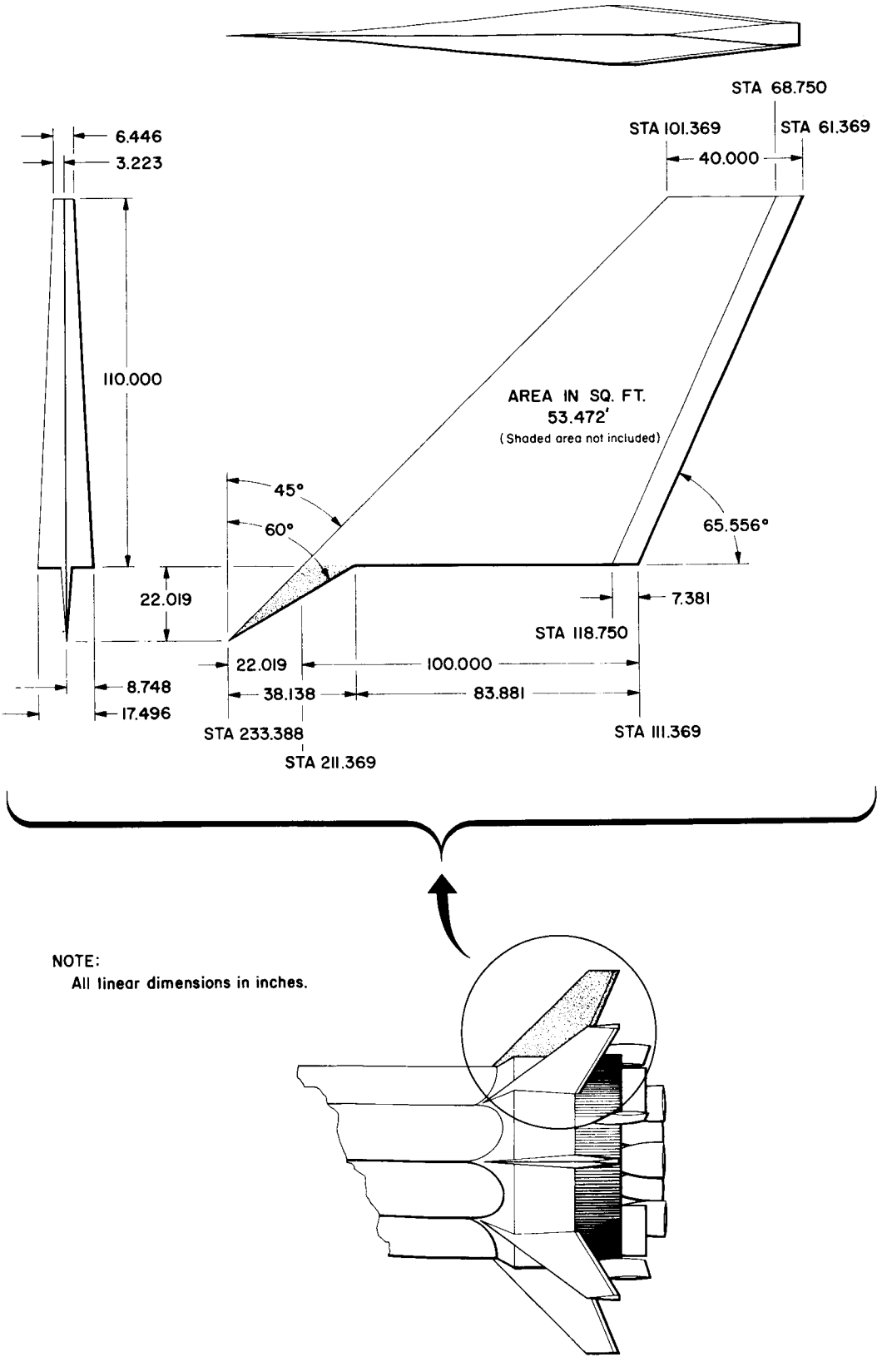

FIGURE 2 GEOMETRY OF THE APOLLO-SATURN IB FIN

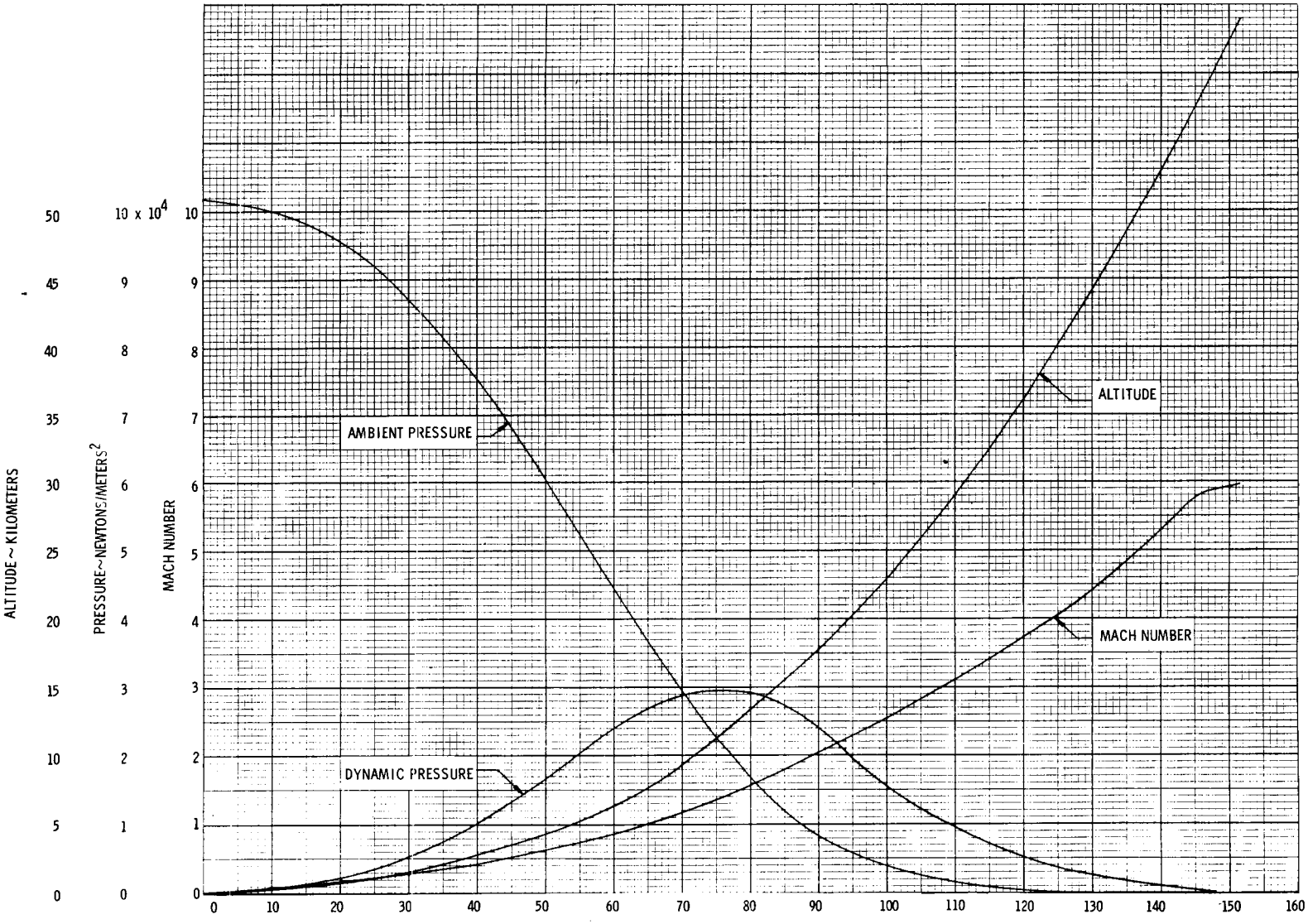

FIGURE 3 TYPICAL APOLLO-SATURN IB TRAJECTORY DATA

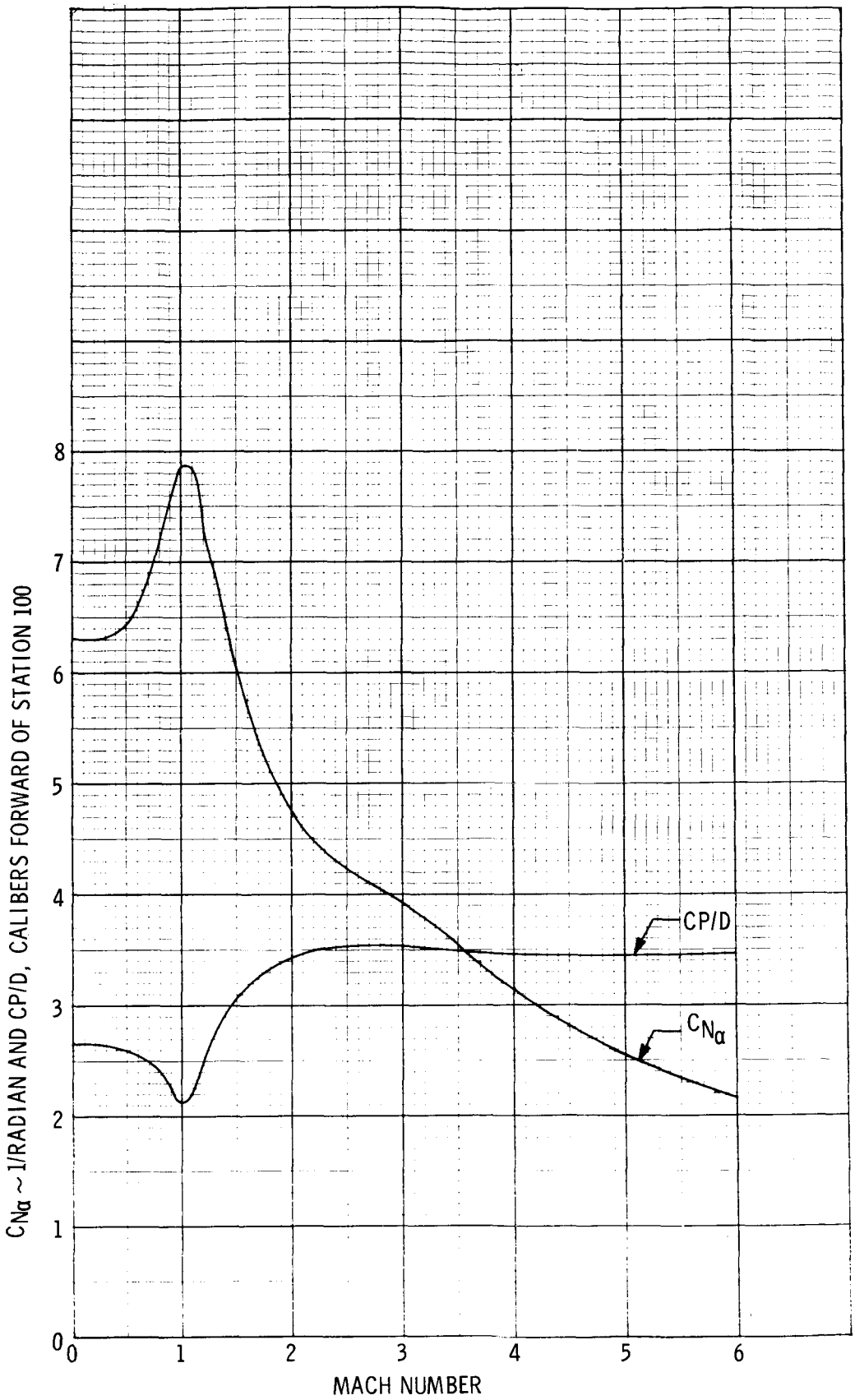

FIGURE 4: VARIATION OF NORMAL FORCE COEFFICIENT GRADIENT AND CENTER OF PRESSURE WITH MACH NUMBER AT $\alpha = 0^0$

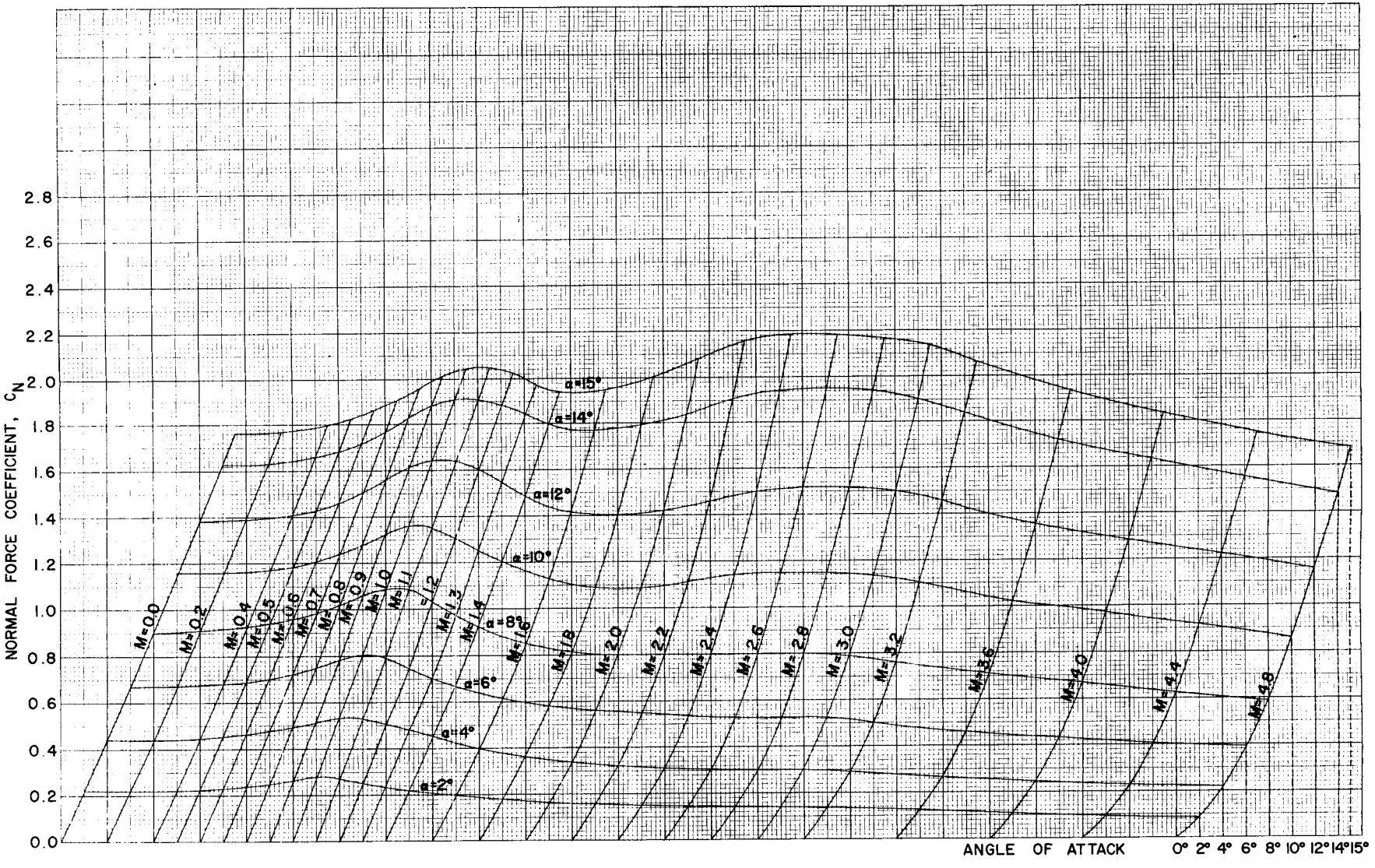

FIGURE 5: VARIATION OF NORMAL FORCE COEFFICIENT WITH ANGLE OF ATTACK AND MACH NUMBER

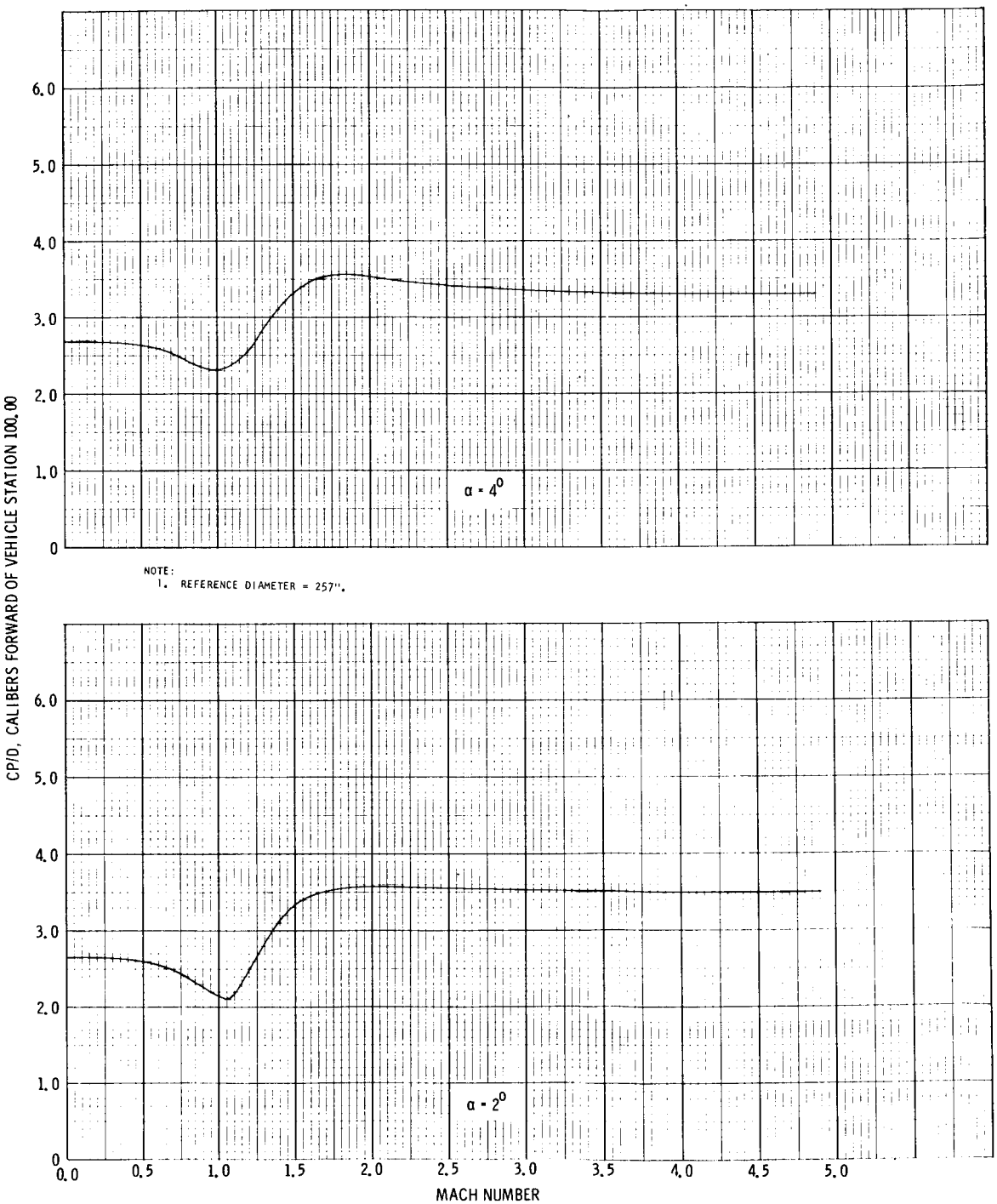

FIGURE 6: VARIATION OF CENTER OF PRESSURE WITH MACH NUMBER AT $\alpha = 2^0$ AND $\alpha = 4^0$.

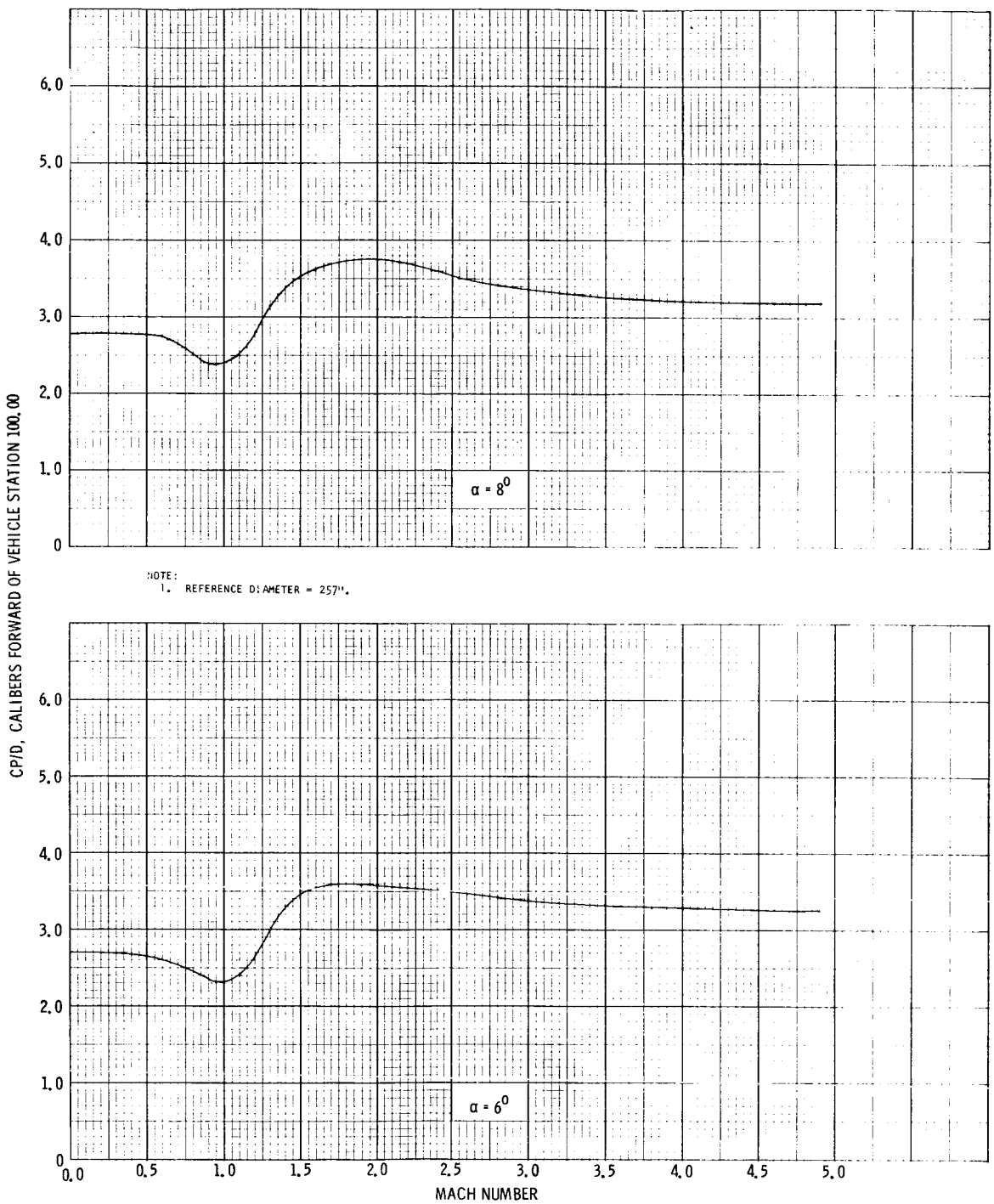

FIGURE 7 VARIATION OF CENTER OF PRESSURE WITH MACH NUMBER AT $\alpha = 6^0$ AND $\alpha = 8^0$.

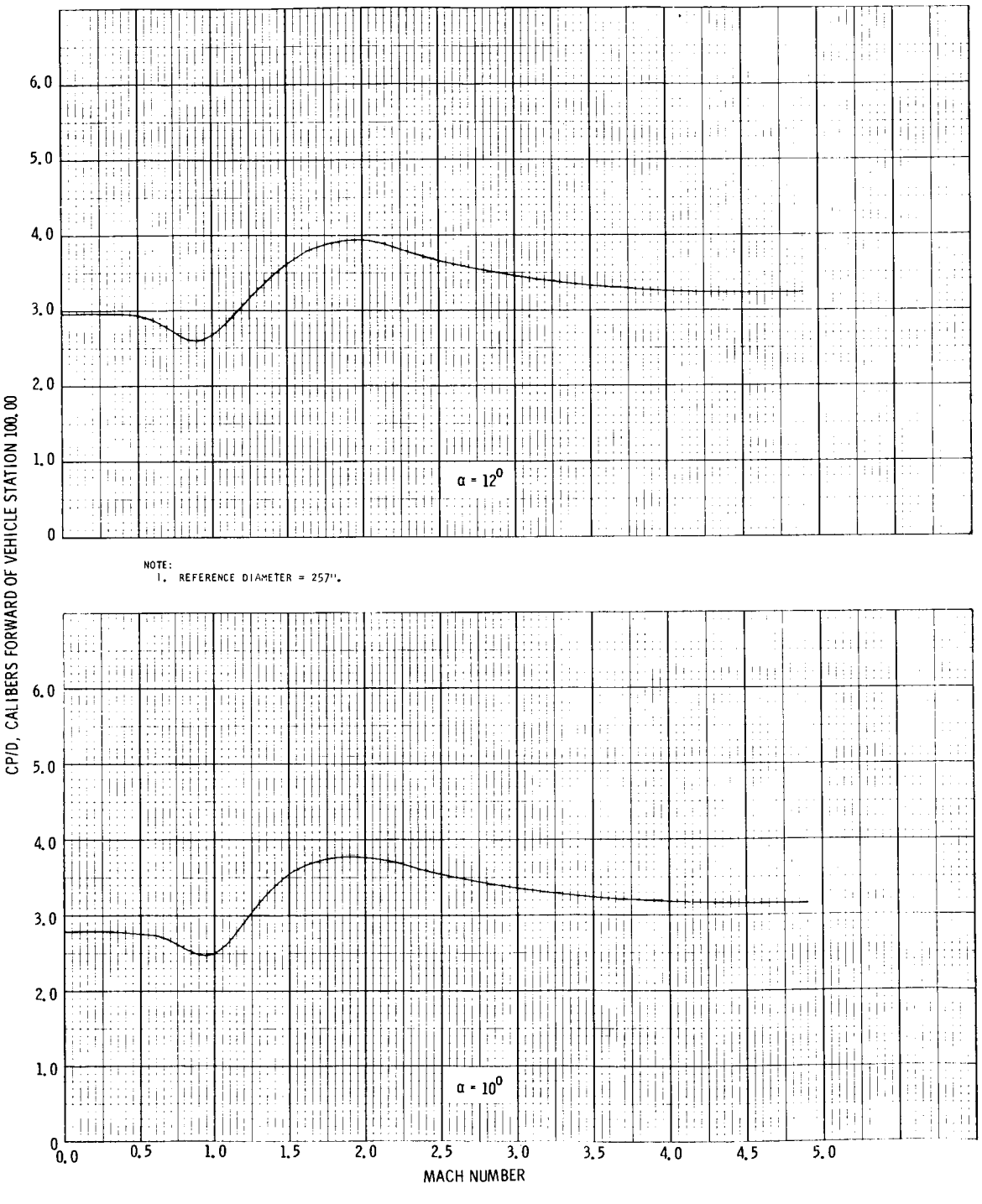

FIGURE 8: VARIATION OF CENTER OF PRESSURE WITH MACH NUMBER AT $\alpha = 10^0$ AND 12^0.

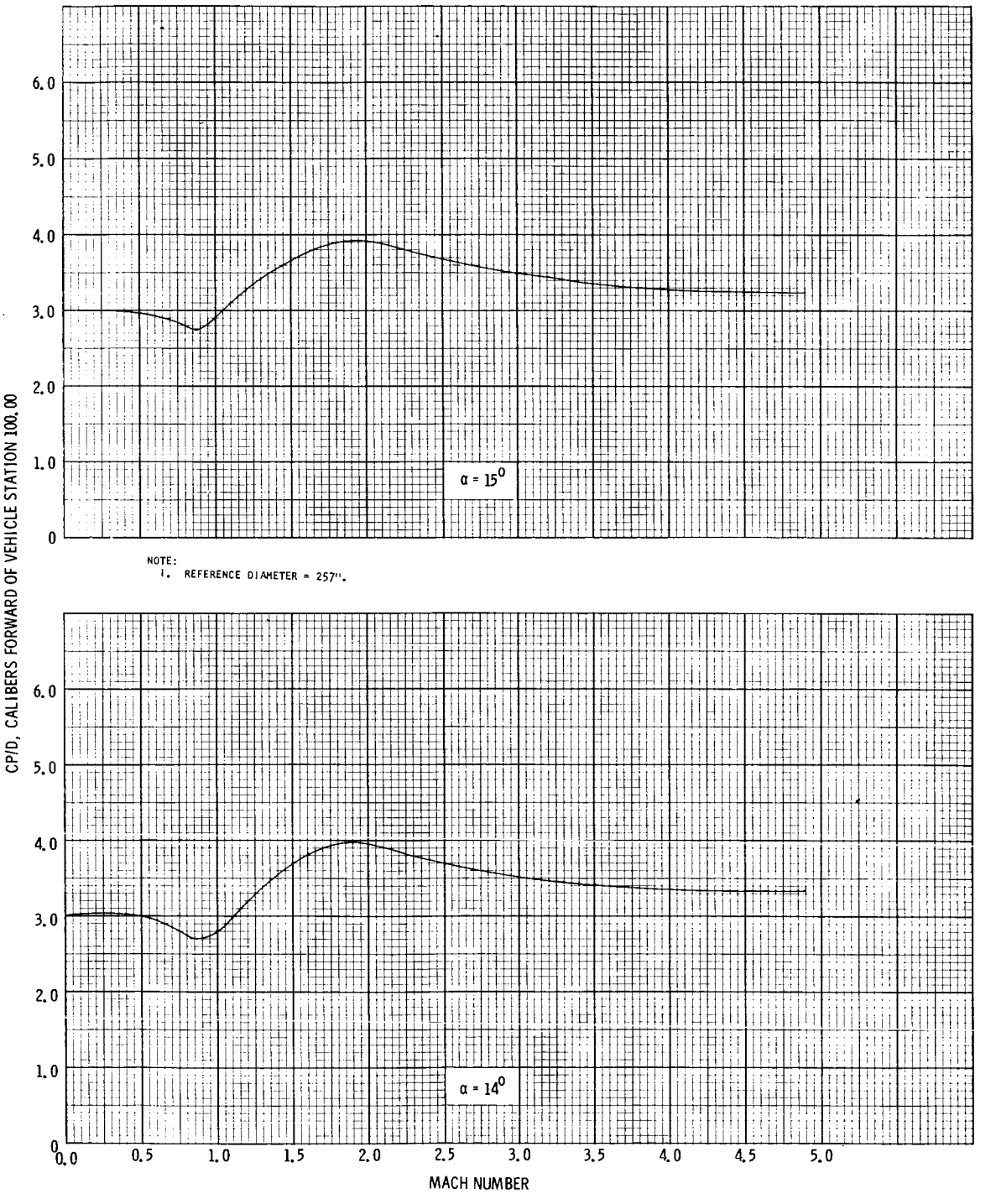

FIGURE 9: VARIATION OF CENTER OF PRESSURE WITH MACH NUMBER AT $\alpha = 14^0$ AND $\alpha = 15^0$.

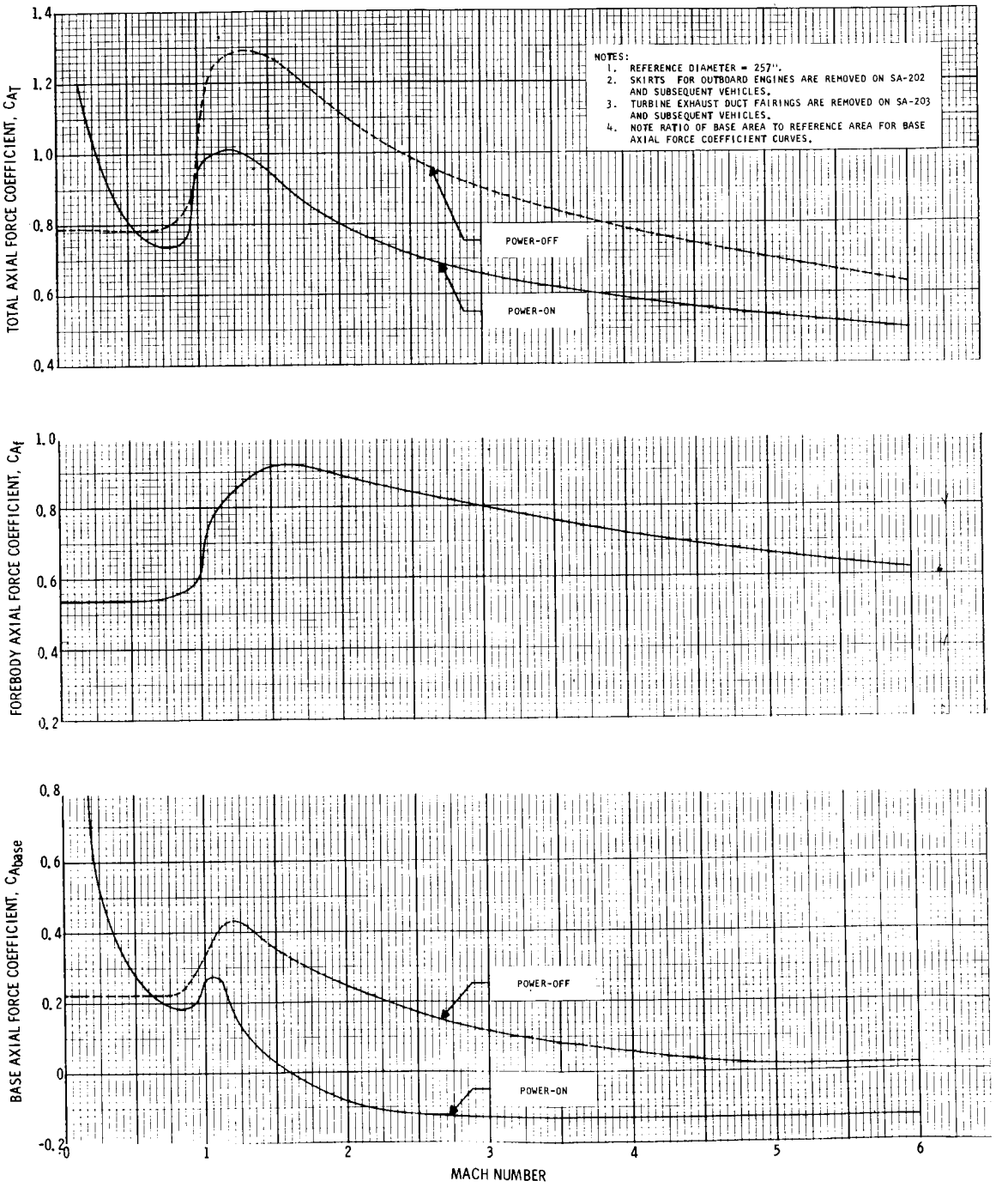

FIGURE 10: VARIATION OF AXIAL FORCE COEFFICIENT WITH MACH NUMBER FOR APOLLO-SATURN 201 AT $\alpha = 0^0$

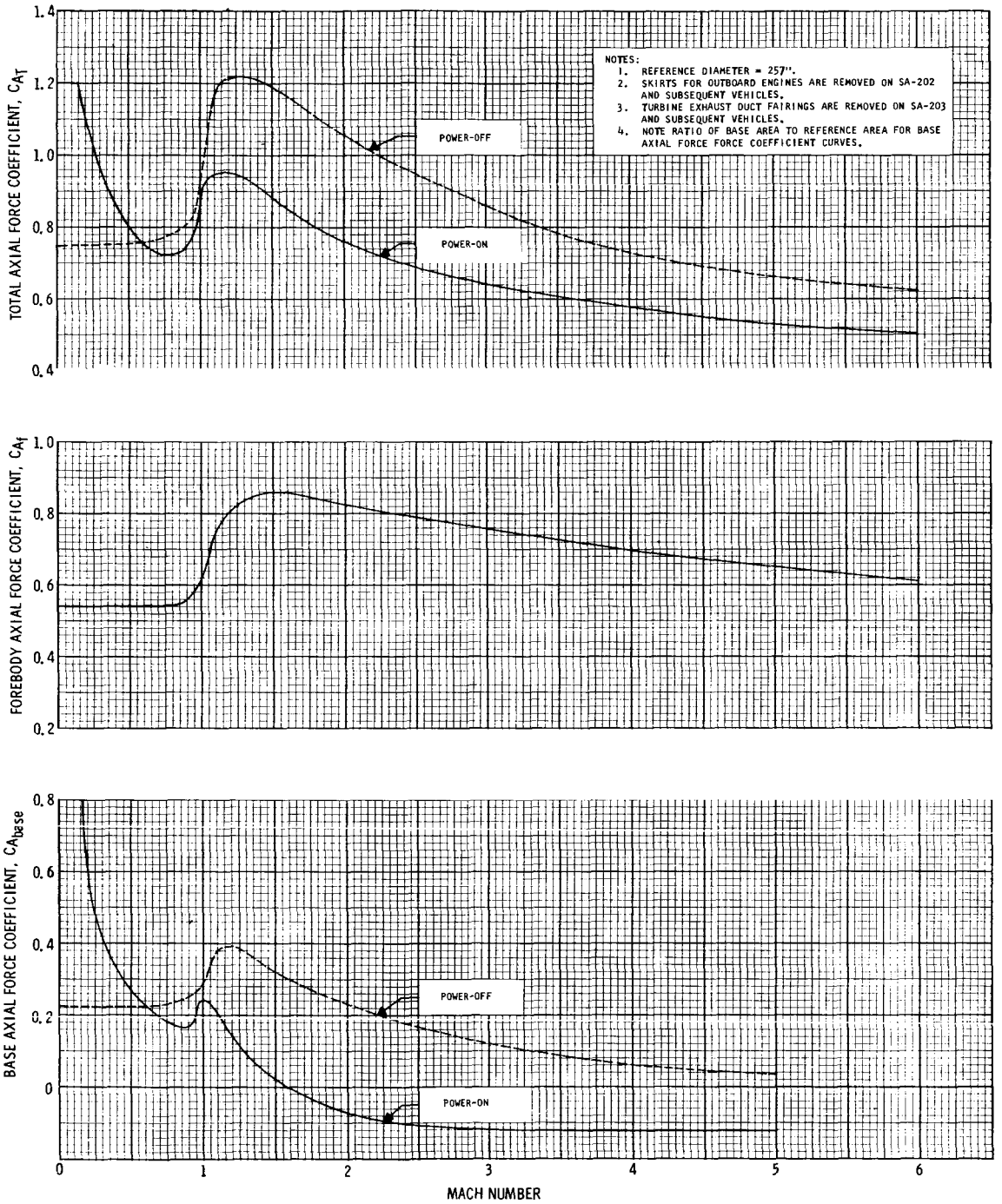

FIGURE 11: VARIATION OF AXIAL FORCE COEFFICIENT WITH MACH NUMBER FOR APOLLO-SATURN 202 AT $\alpha = 0^0$

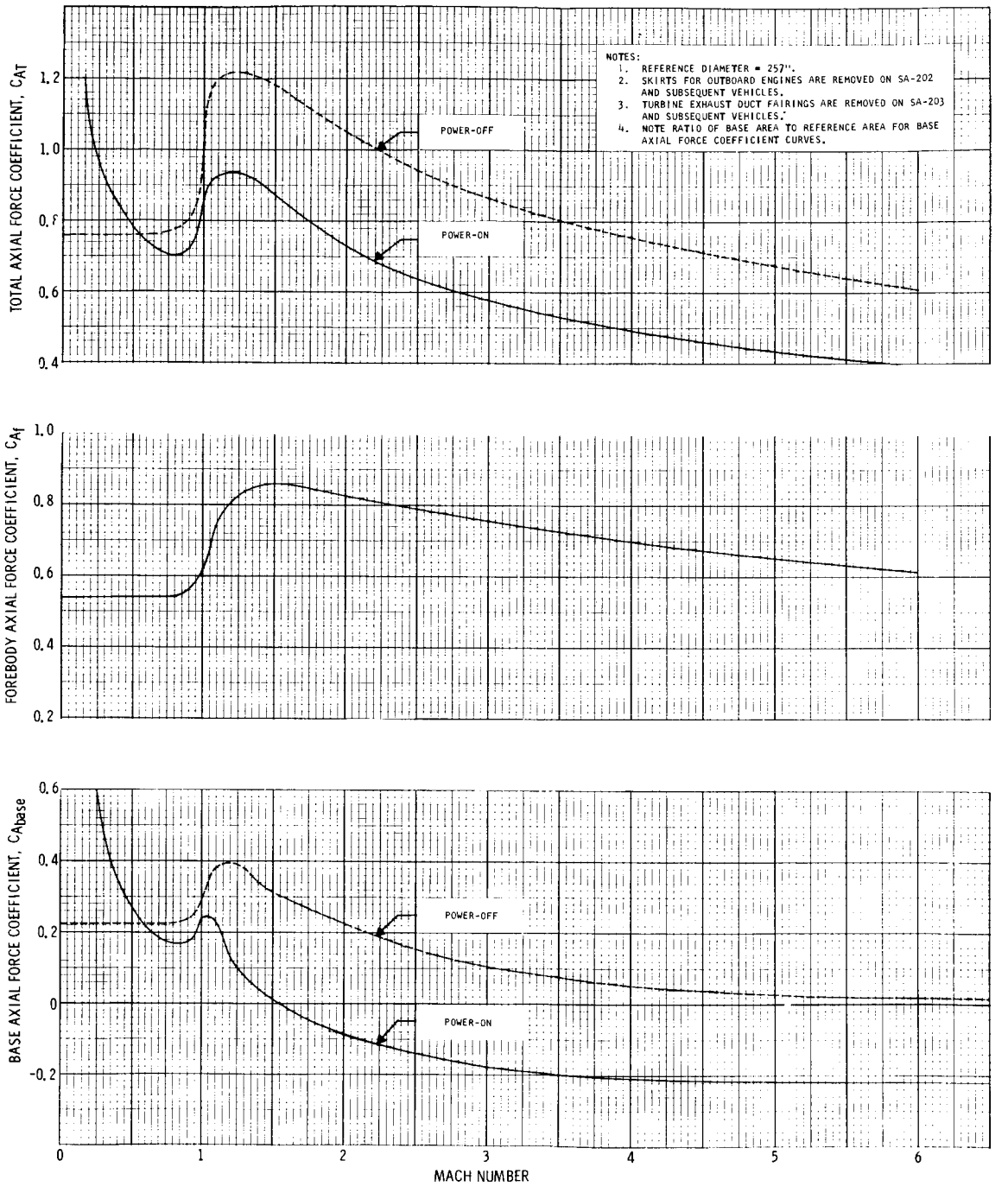

FIGURE 12: VARIATION OF AXIAL FORCE COEFFICIENT WITH MACH NUMBER FOR APOLLO-SATURN 204 AND SUBSEQUENT VEHICLES AT $\alpha = 0^0$

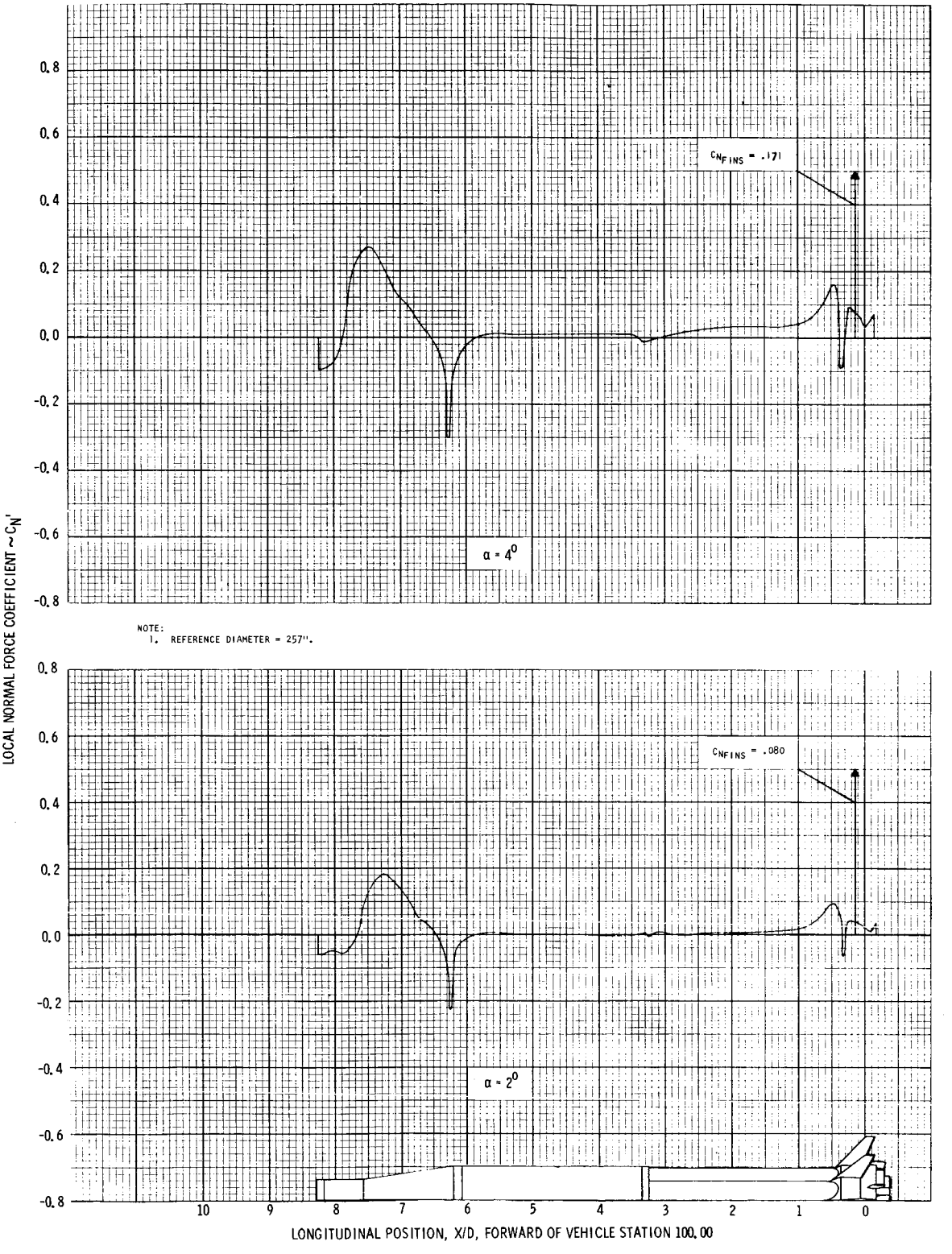

FIGURE 13: DISTRIBUTION OF LOCAL NORMAL FORCE COEFFICIENT AT MACH 0.5; α = 2° AND 4°.

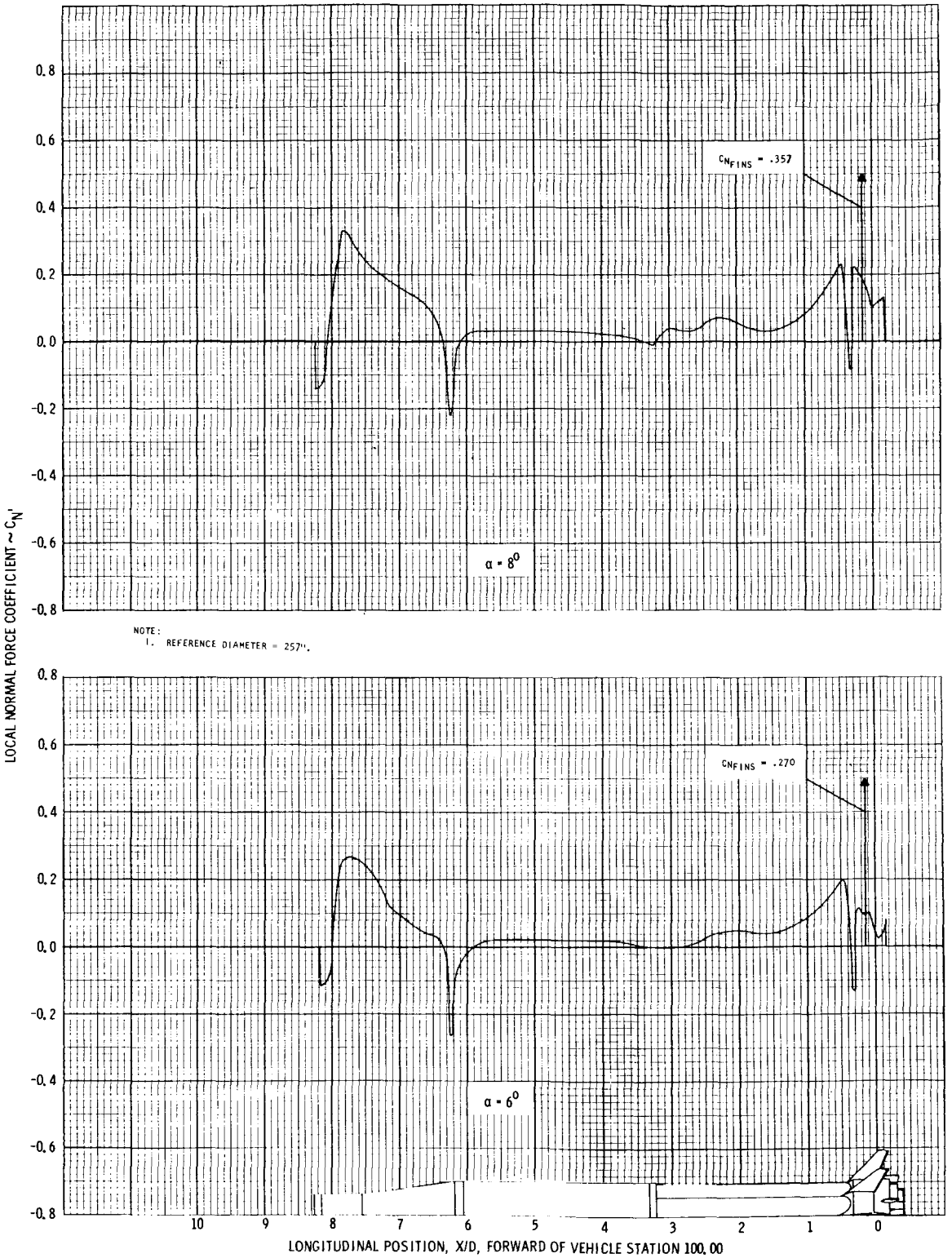

FIGURE 14: DISTRIBUTION OF LOCAL NORMAL FORCE COEFFICIENT AT MACH 0.5; α = 6° AND 8°.

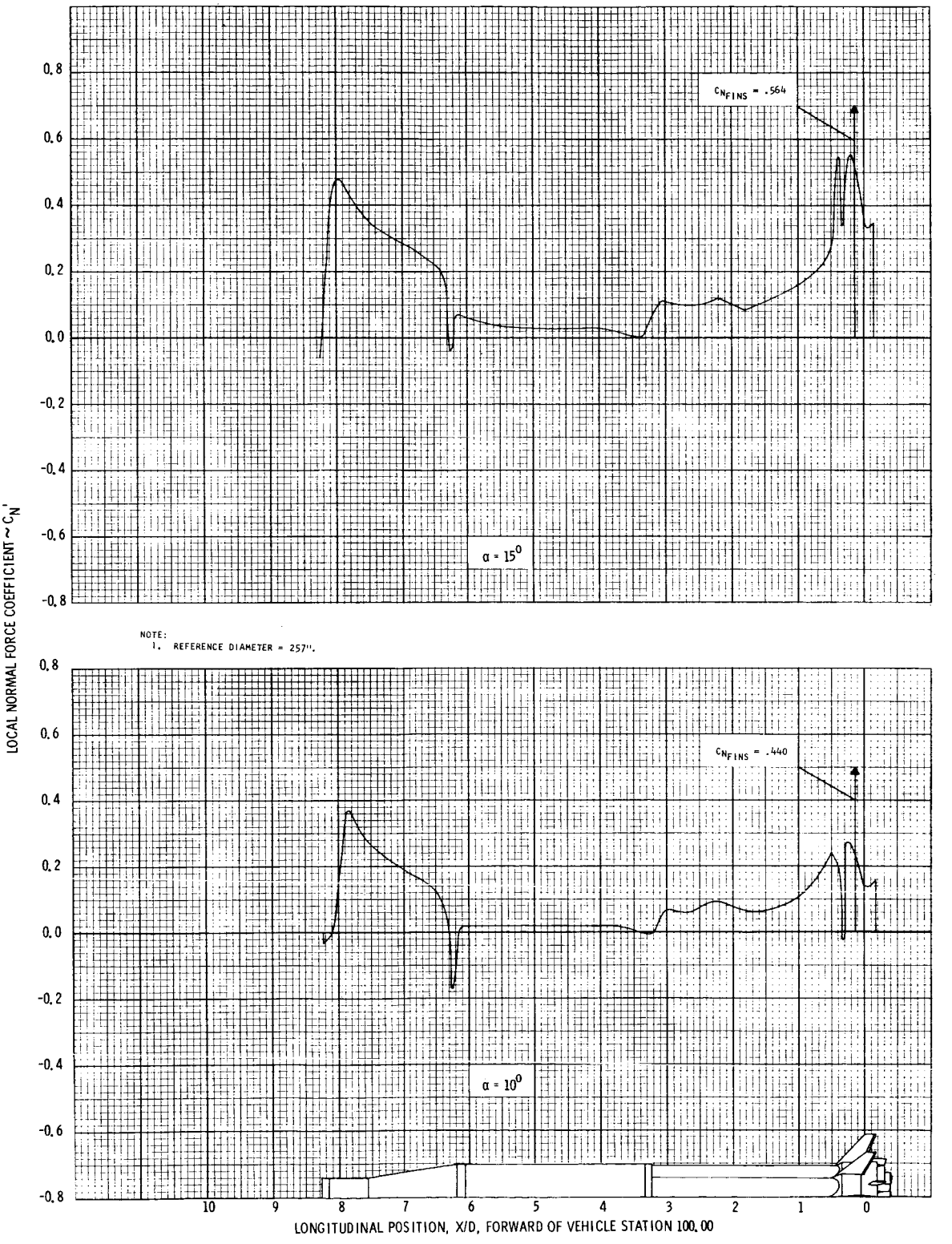

NOTE:
1. REFERENCE DIAMETER = 257".

FIGURE 15: DISTRIBUTION OF LOCAL NORMAL FORCE COEFFICIENT AT MACH 0.5; α = 10° AND 15°.

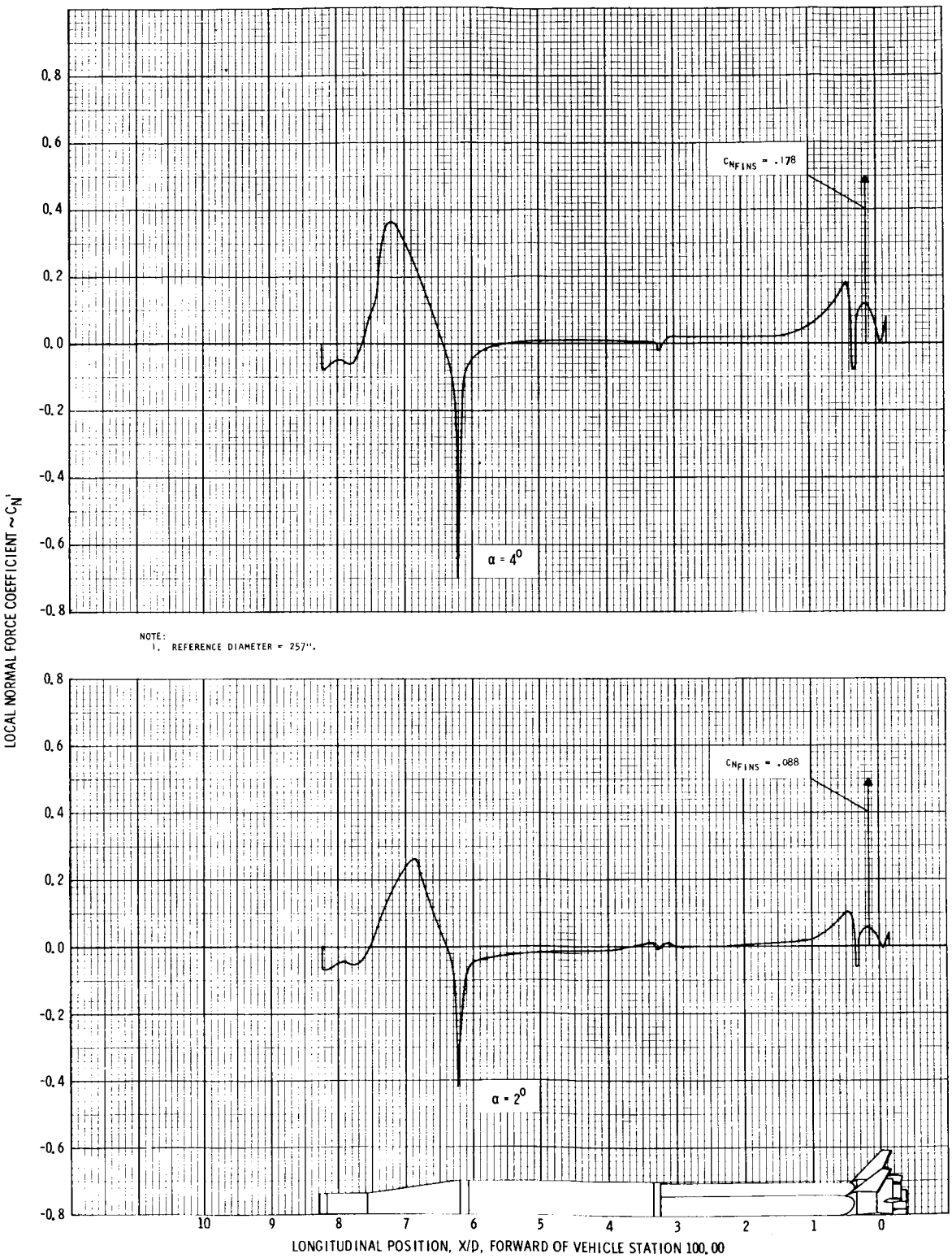

FIGURE 16: DISTRIBUTION OF LOCAL NORMAL FORCE COEFFICIENT AT MACH 0.8; α = 2° AND 4°.

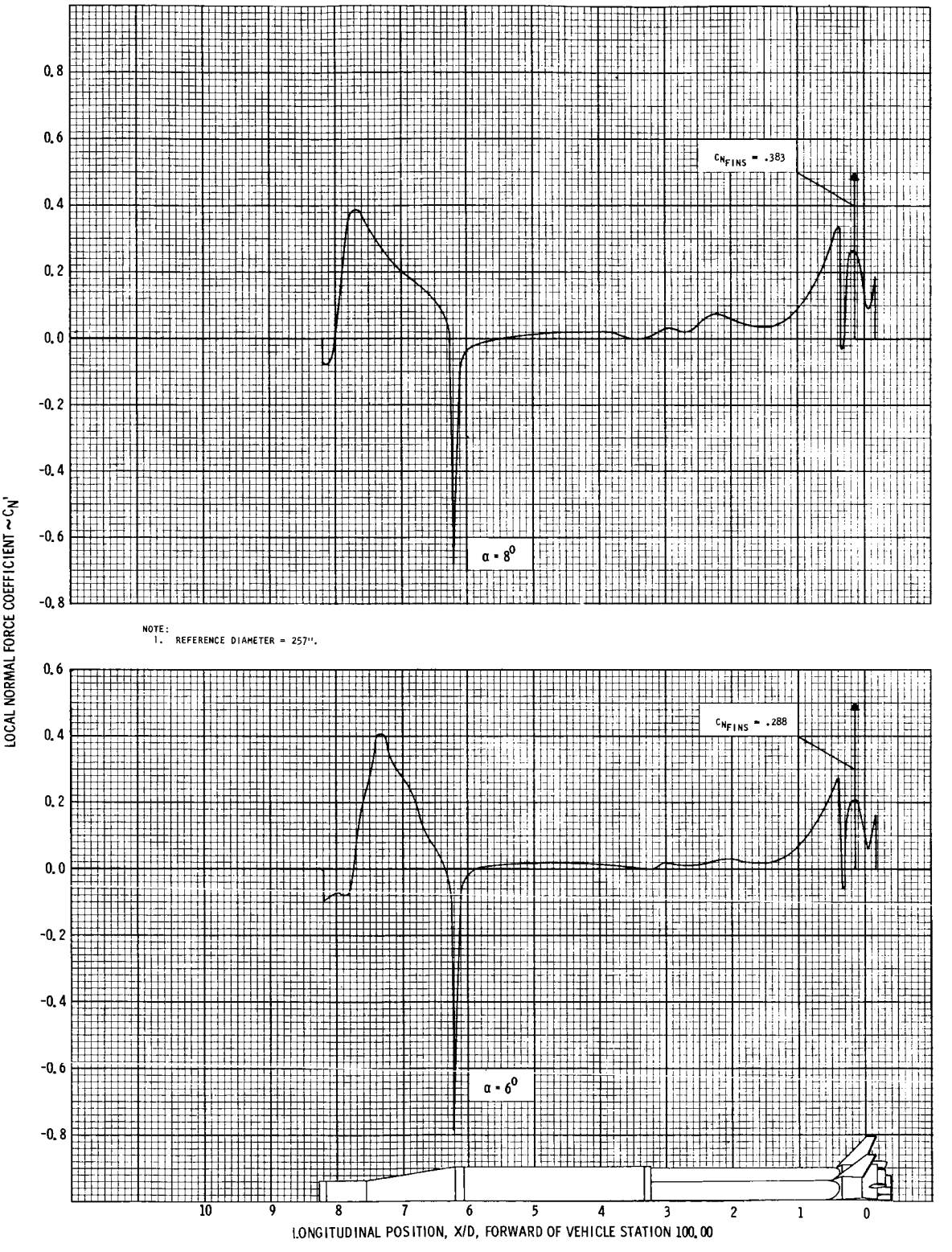

FIGURE 17: DISTRIBUTION OF LOCAL NORMAL FORCE COEFFICIENT AT MACH 0.8; $\alpha = 6^0$ AND 8^0.

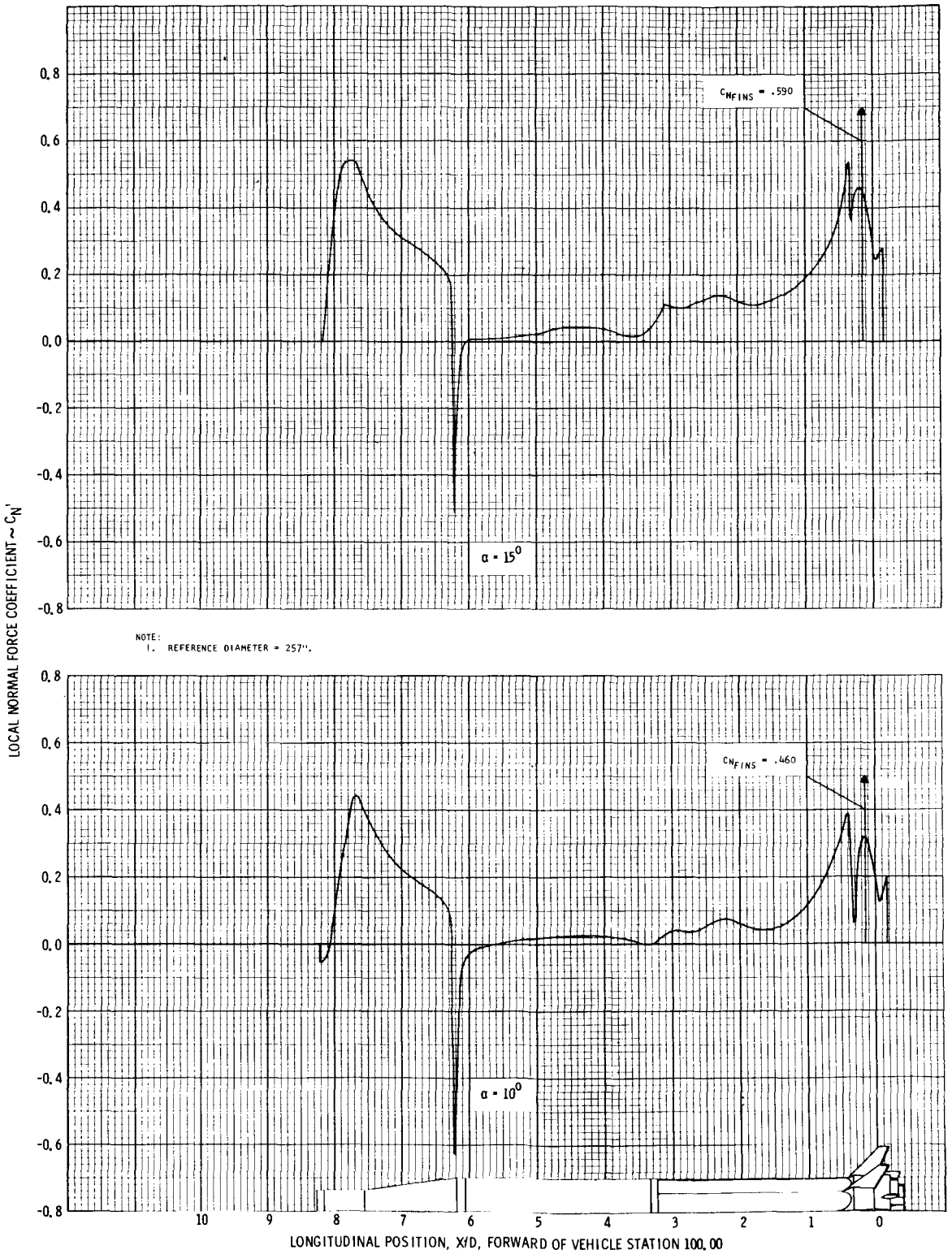

NOTE:
1. REFERENCE DIAMETER = 257".

FIGURE 18: DISTRIBUTION OF LOCAL NORMAL FORCE COEFFICIENT AT MACH 0.8; α = 10° AND 15°.

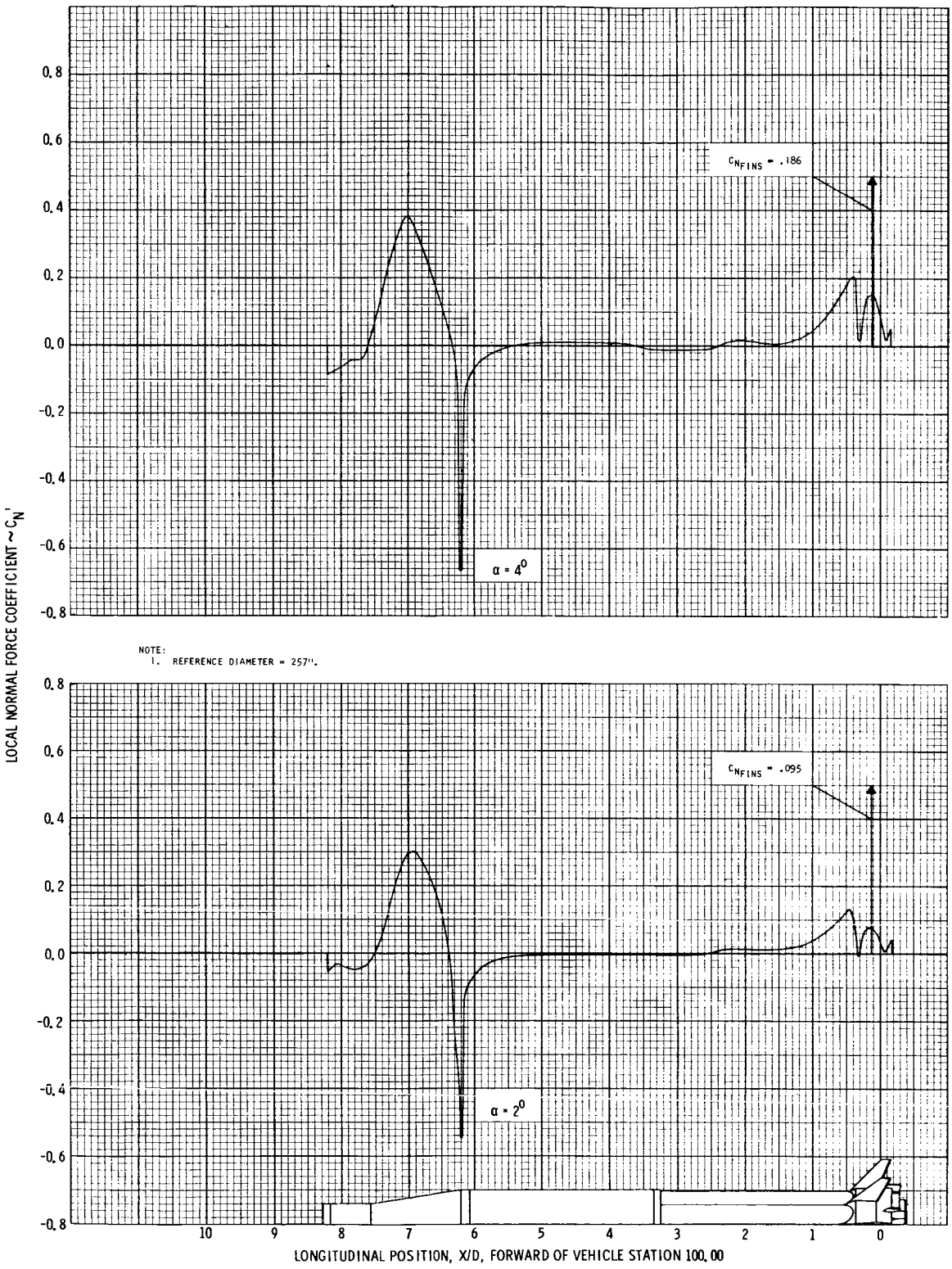

FIGURE 19: DISTRIBUTION OF LOCAL NORMAL FORCE COEFFICIENT AT MACH 0.9; α = 2° AND 4°.

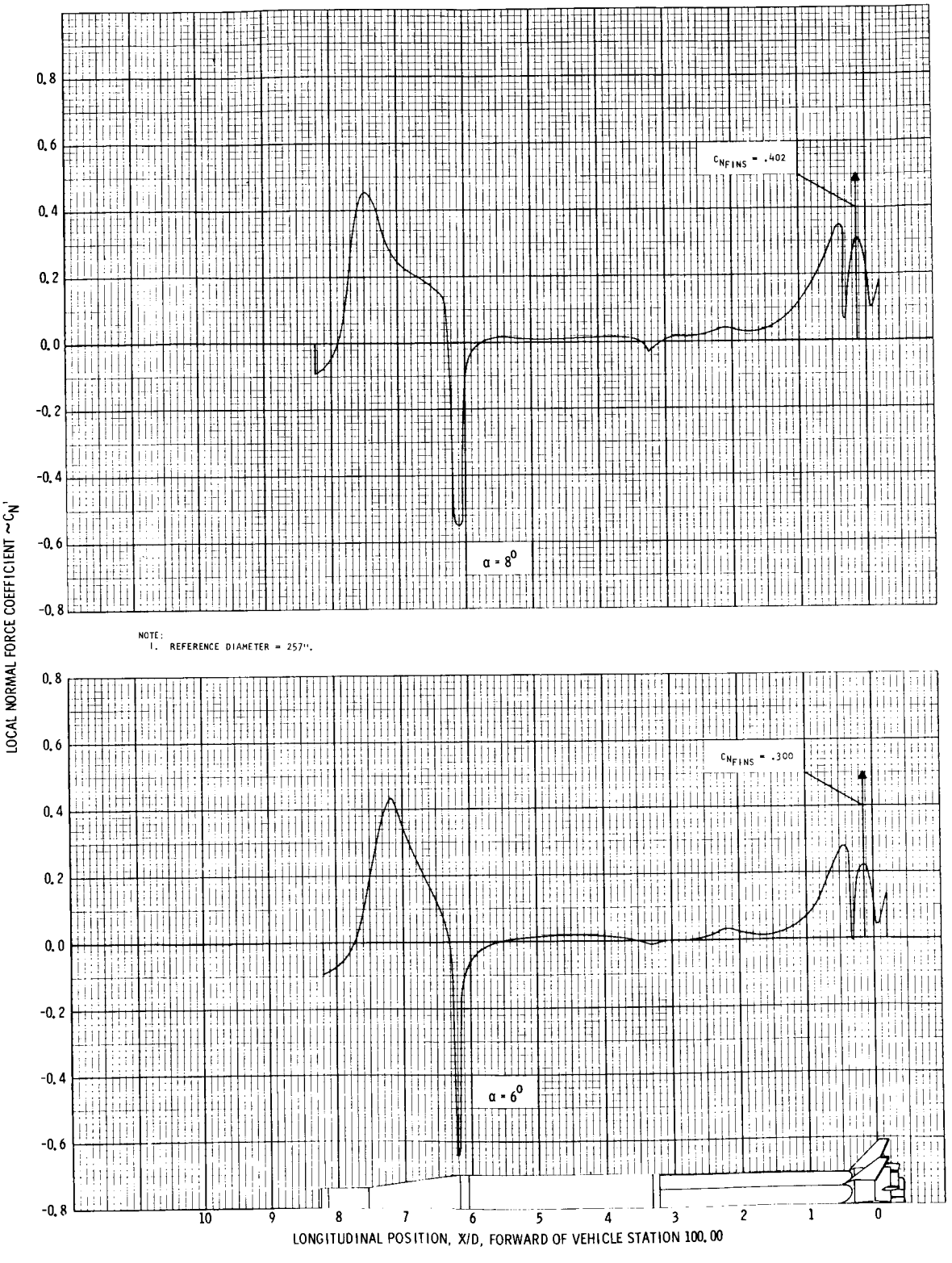

FIGURE 20: DISTRIBUTION OF LOCAL NORMAL FORCE COEFFICIENT AT MACH 0.9; α = 6° AND 8°.

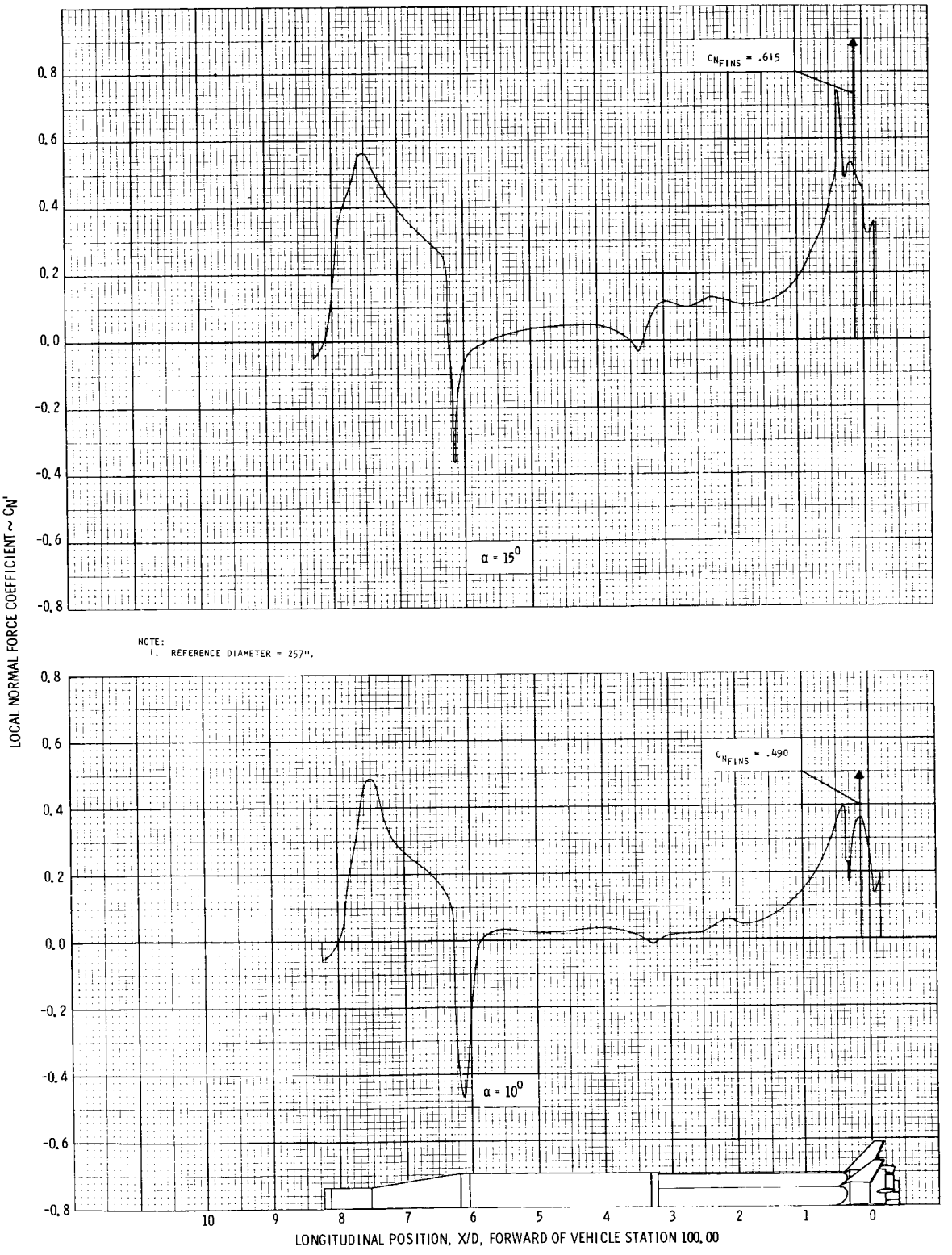

NOTE:
1. REFERENCE DIAMETER = 257".

FIGURE 21: DISTRIBUTION OF LOCAL NORMAL FORCE COEFFICIENT AT MACH 0.9; $\alpha = 10^0$ AND 15^0.

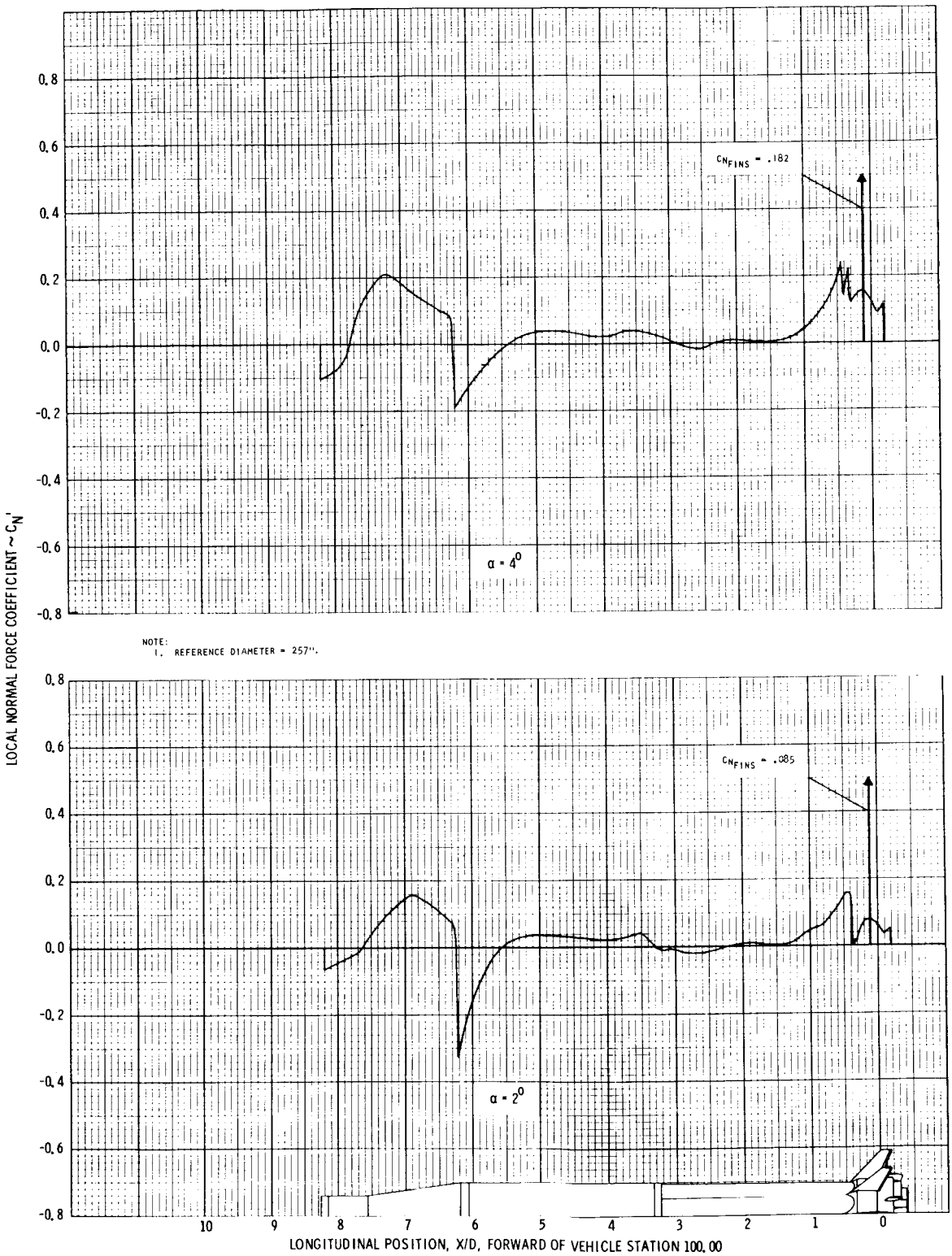

FIGURE 22: DISTRIBUTION OF LOCAL NORMAL FORCE COEFFICIENT AT MACH 1.0; α = 2° AND 4°.

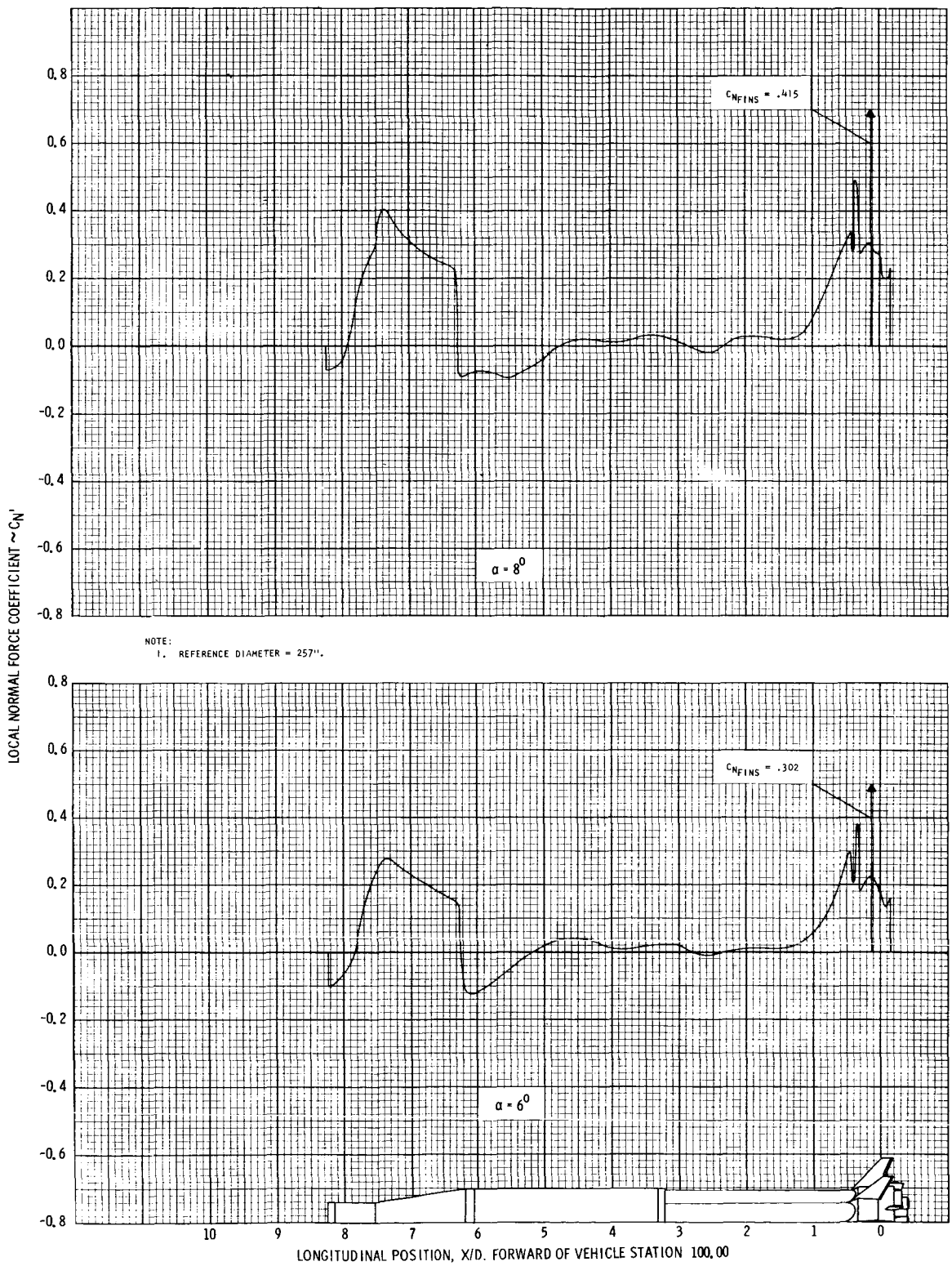

FIGURE 23: DISTRIBUTION OF LOCAL NORMAL FORCE COEFFICIENT AT MACH 1.0; α = 6° AND 8°.

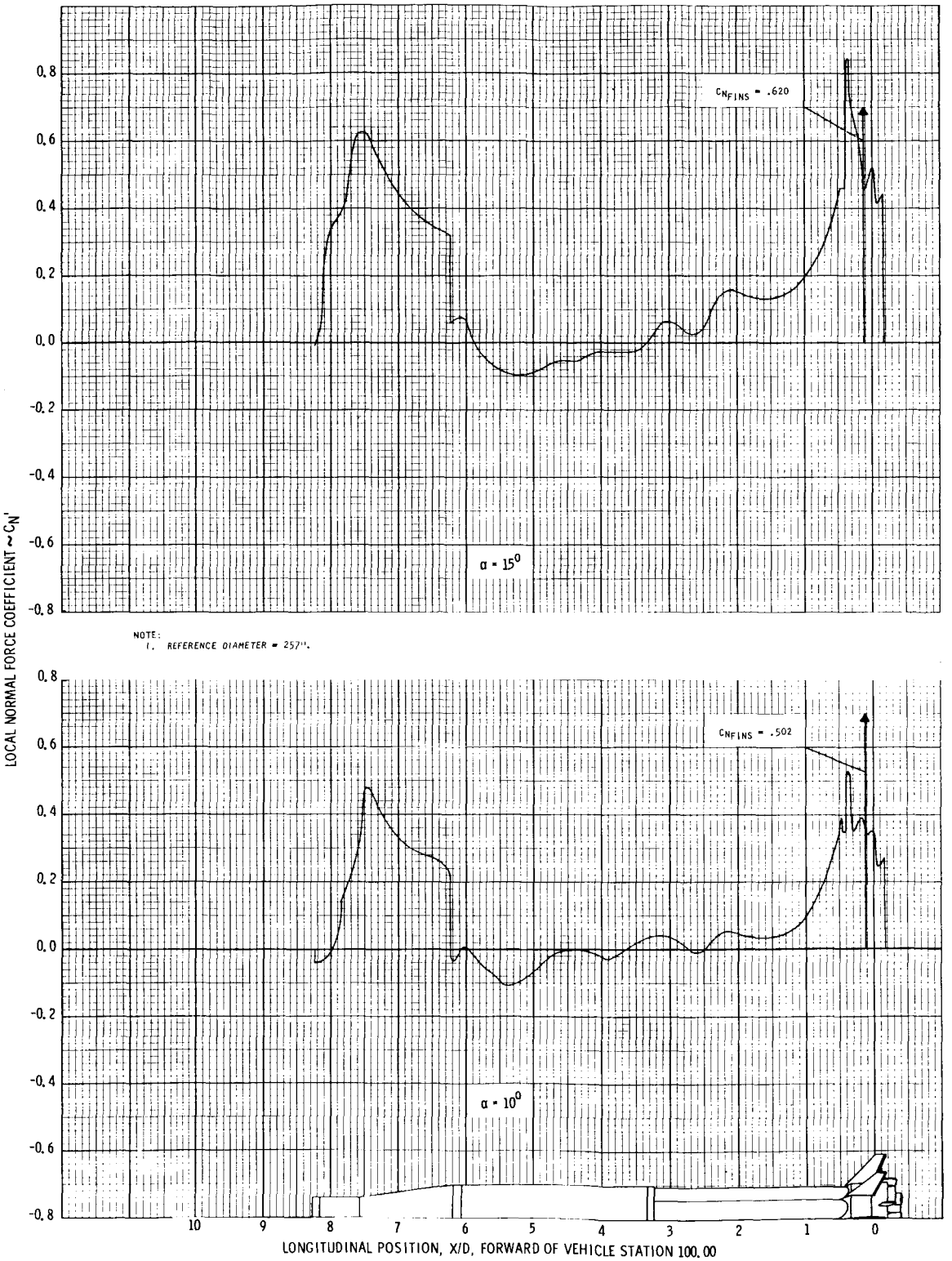

FIGURE 24: DISTRIBUTION OF LOCAL NORMAL FORCE COEFFICIENT AT MACH 1.0; α = 10° AND 15°.

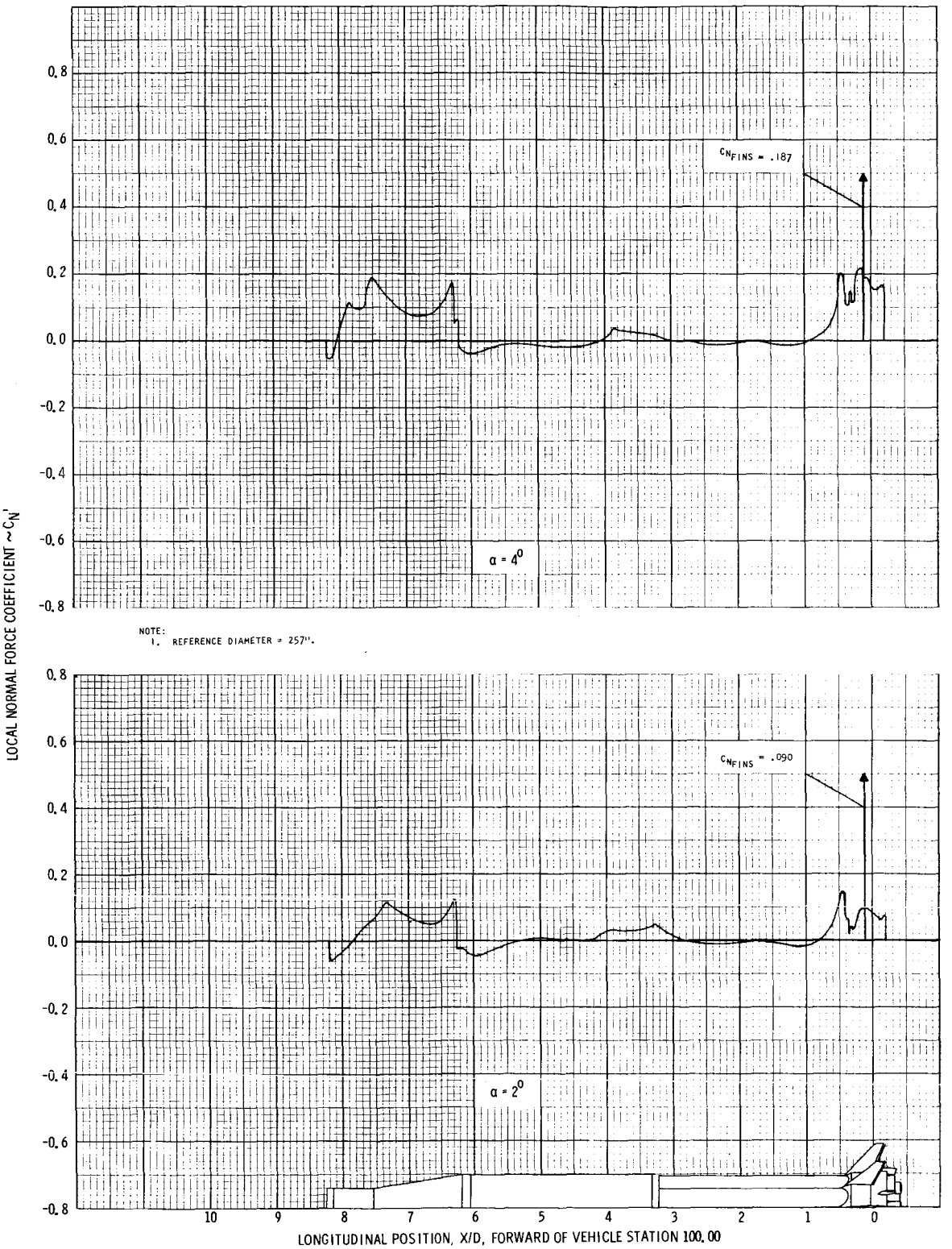

FIGURE 25: DISTRIBUTION OF LOCAL NORMAL FORCE COEFFICIENT AT MACH 1.2; $\alpha = 2^0$ AND 4^0.

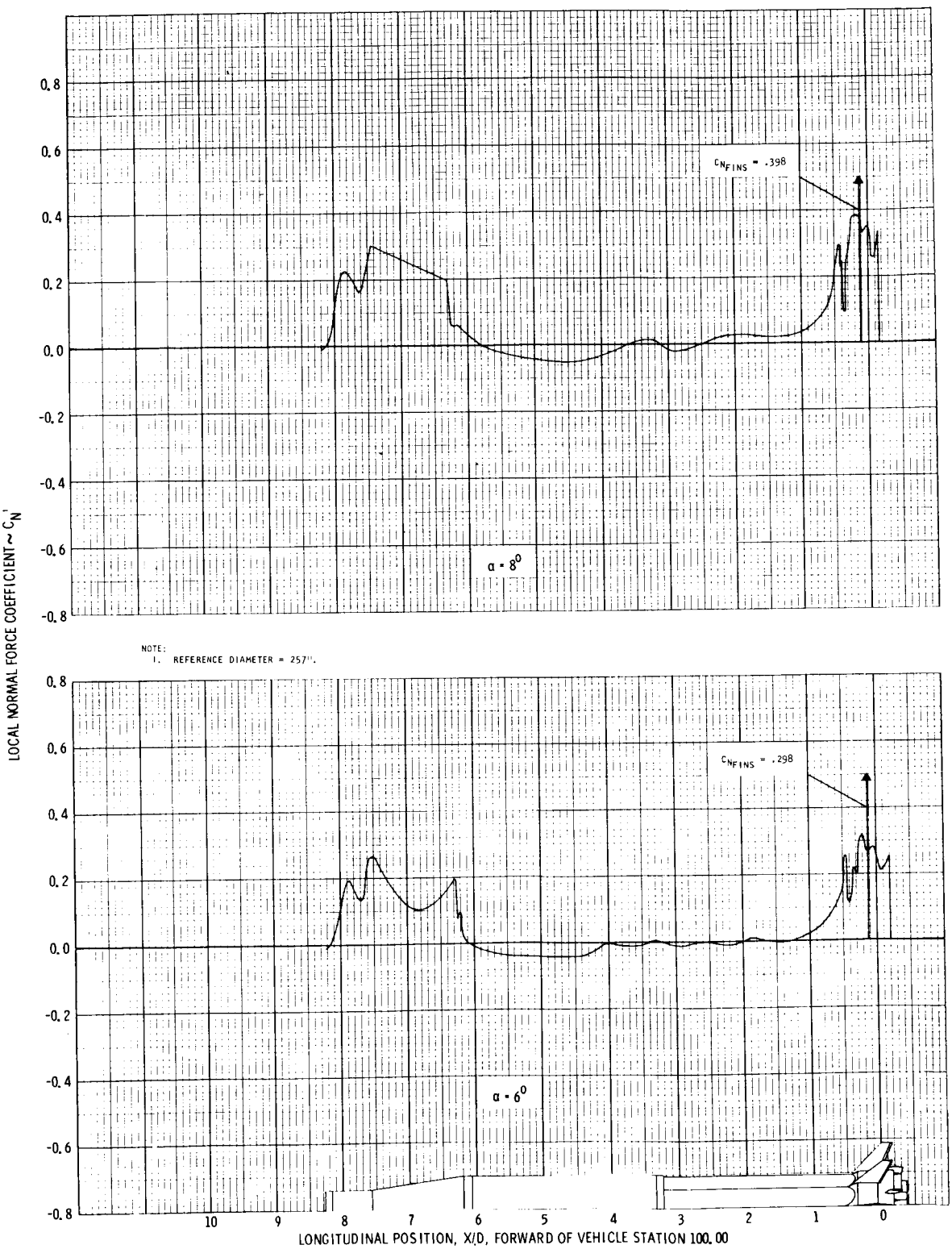

FIGURE 26: DISTRIBUTION OF LOCAL NORMAL FORCE COEFFICIENT AT MACH 1.2; α = 6° AND 8°.

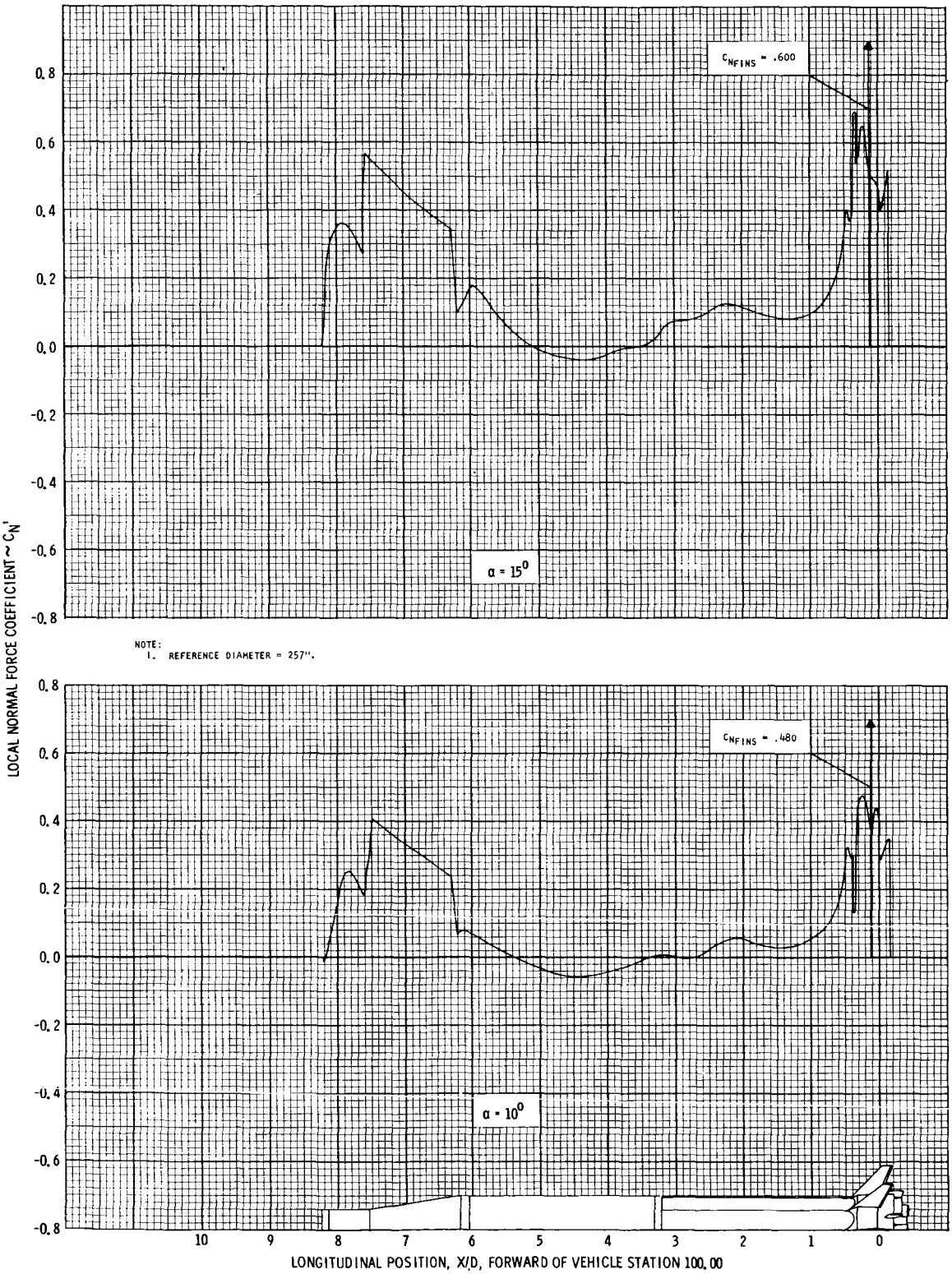

FIGURE 27: DISTRIBUTION OF LOCAL NORMAL FORCE COEFFICIENT AT MACH 1.2; α = 10° AND 15°.

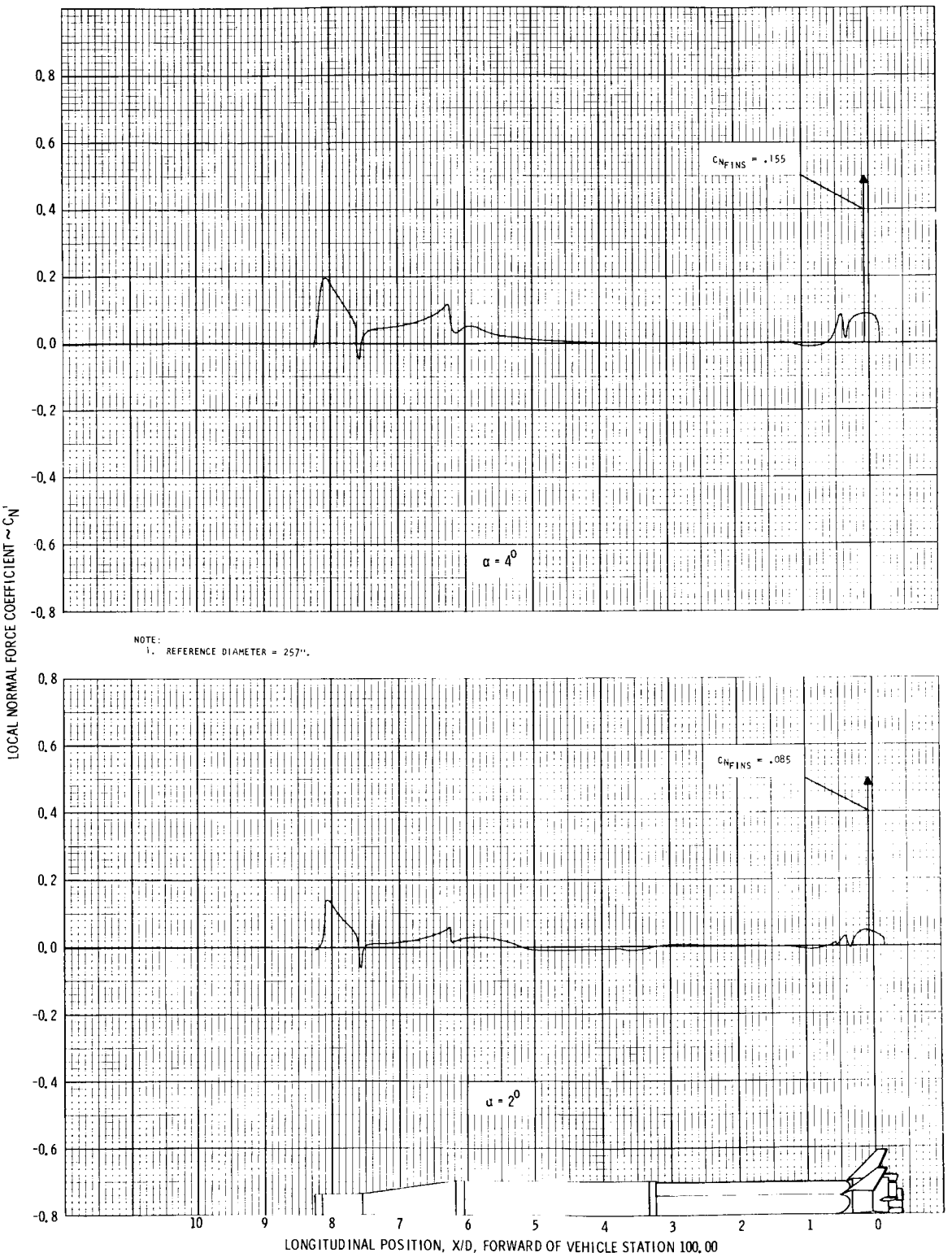

FIGURE 28: DISTRIBUTION OF LOCAL NORMAL FORCE COEFFICIENT AT MACH 1.57; α = 2° AND 4°.

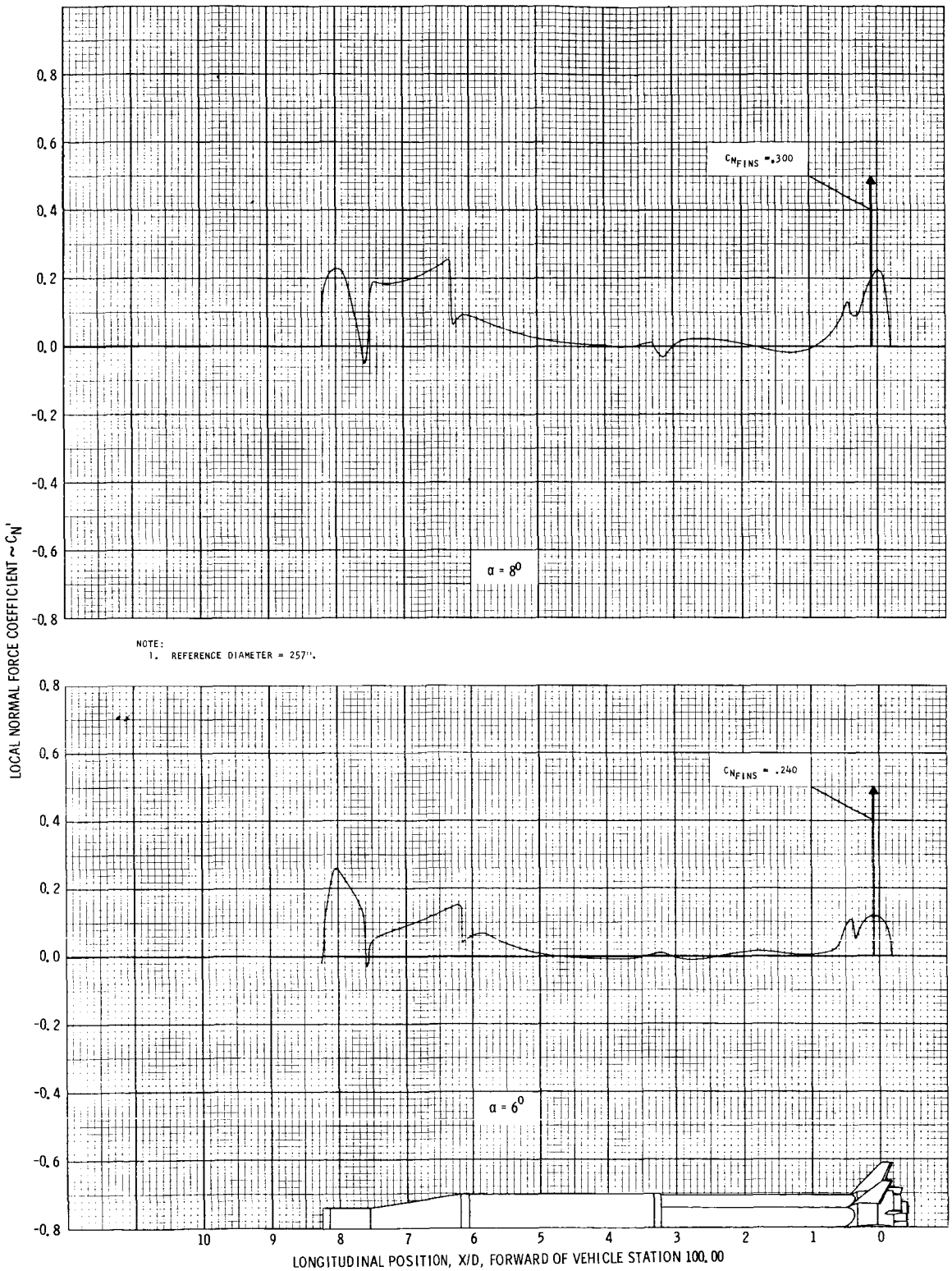

FIGURE 29: DISTRIBUTION OF LOCAL NORMAL FORCE COEFFICIENT AT MACH 1.57; $\alpha = 6^0$ AND 8^0.

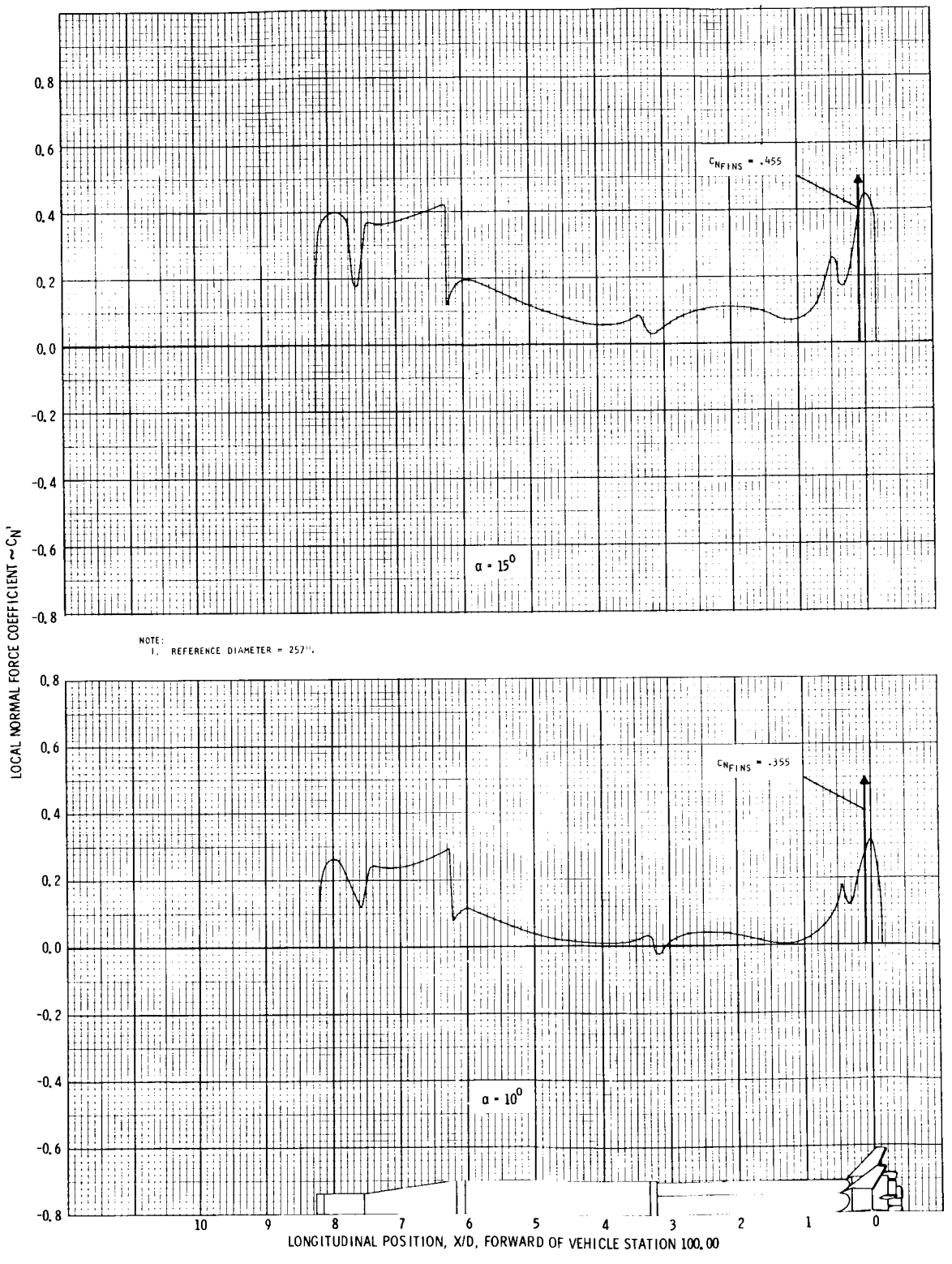

FIGURE 30: DISTRIBUTION OF LOCAL NORMAL FORCE COEFFICIENT AT MACH 1.57; α = 10° AND 15°.

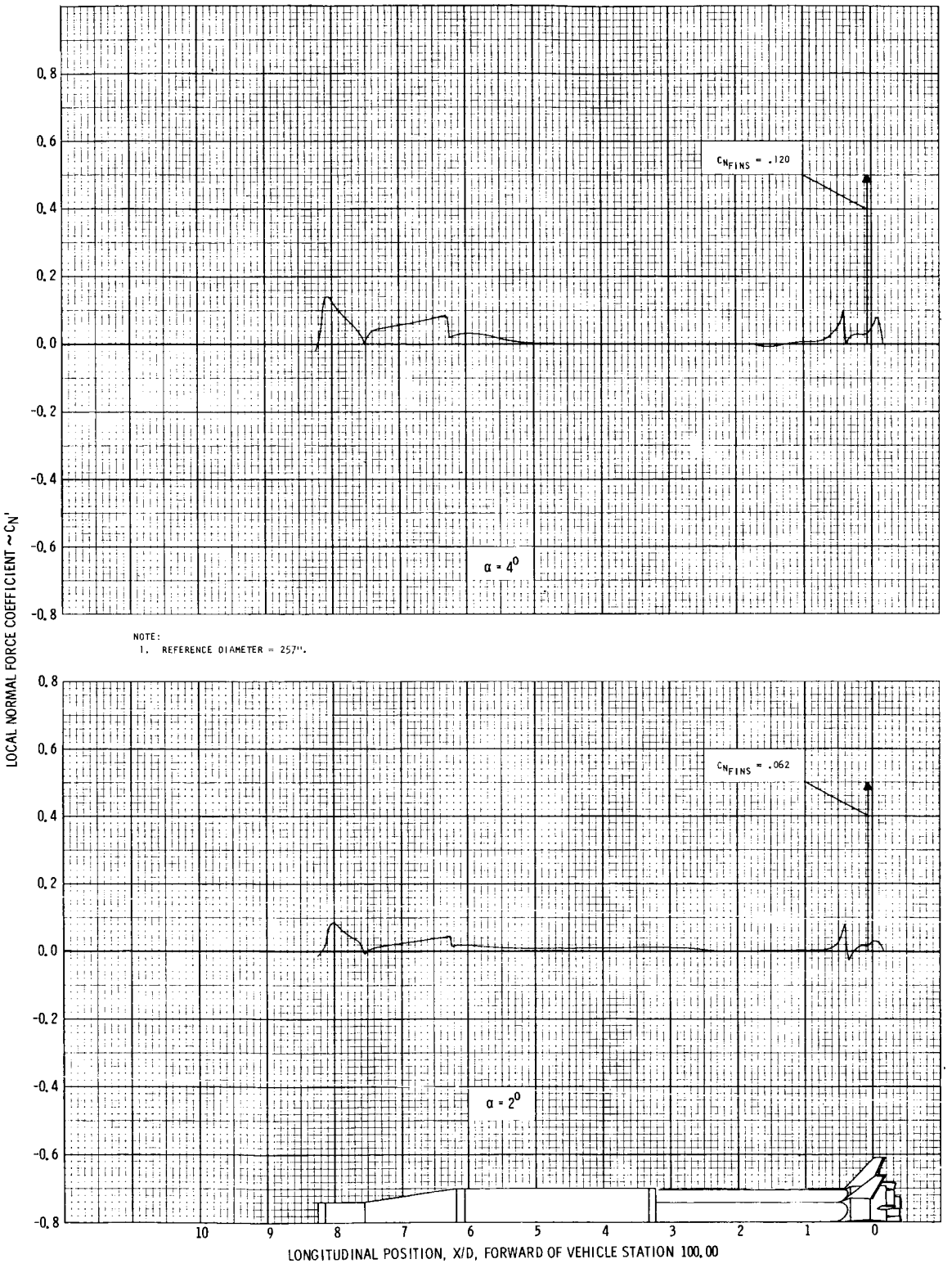

FIGURE 31: DISTRIBUTION OF LOCAL NORMAL FORCE COEFFICIENT AT MACH 2.16; α = 2^0 AND 4^0.

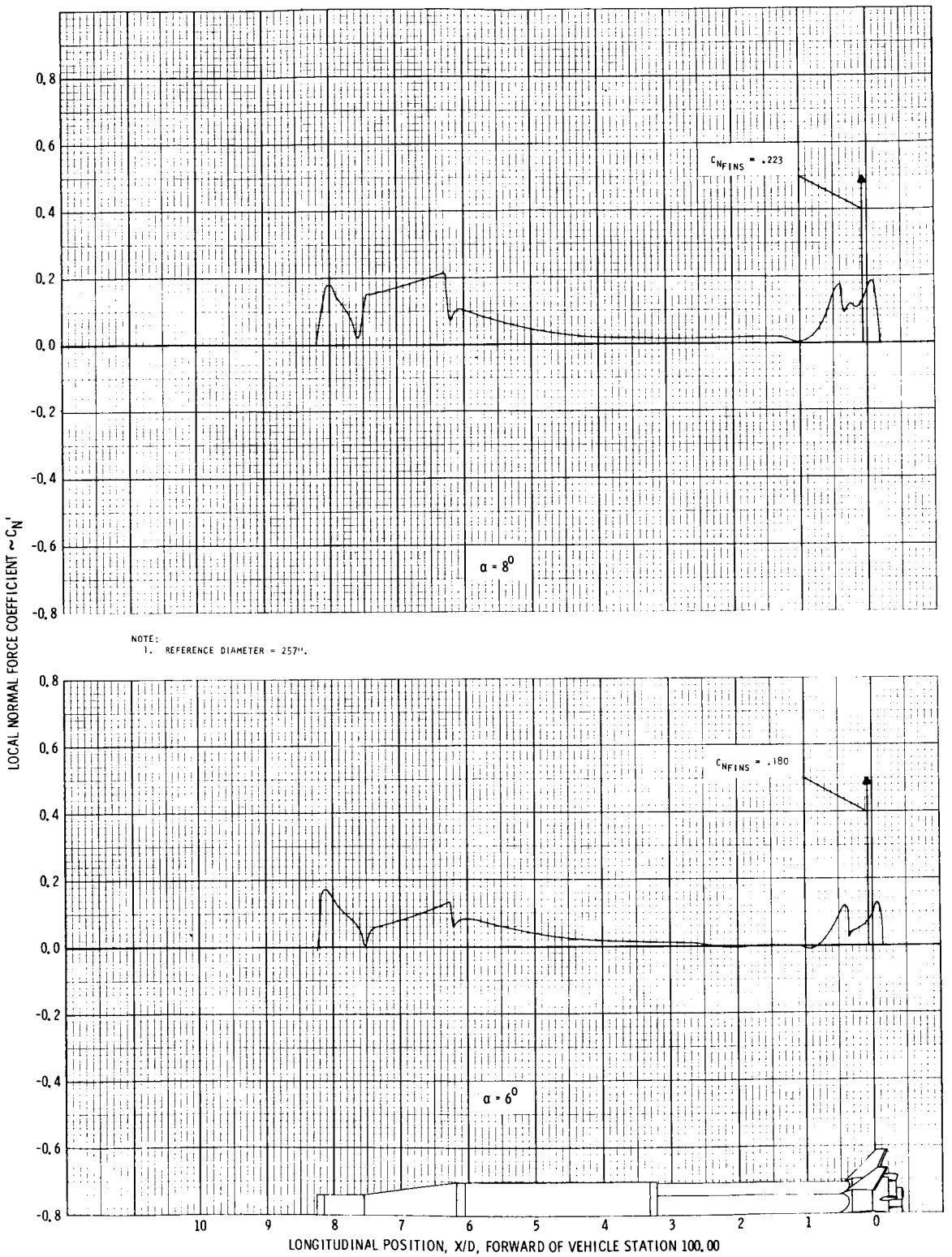

FIGURE 32: DISTRIBUTION OF LOCAL NORMAL FORCE COEFFICIENT AT MACH 2.16; α = 6° AND 8°.

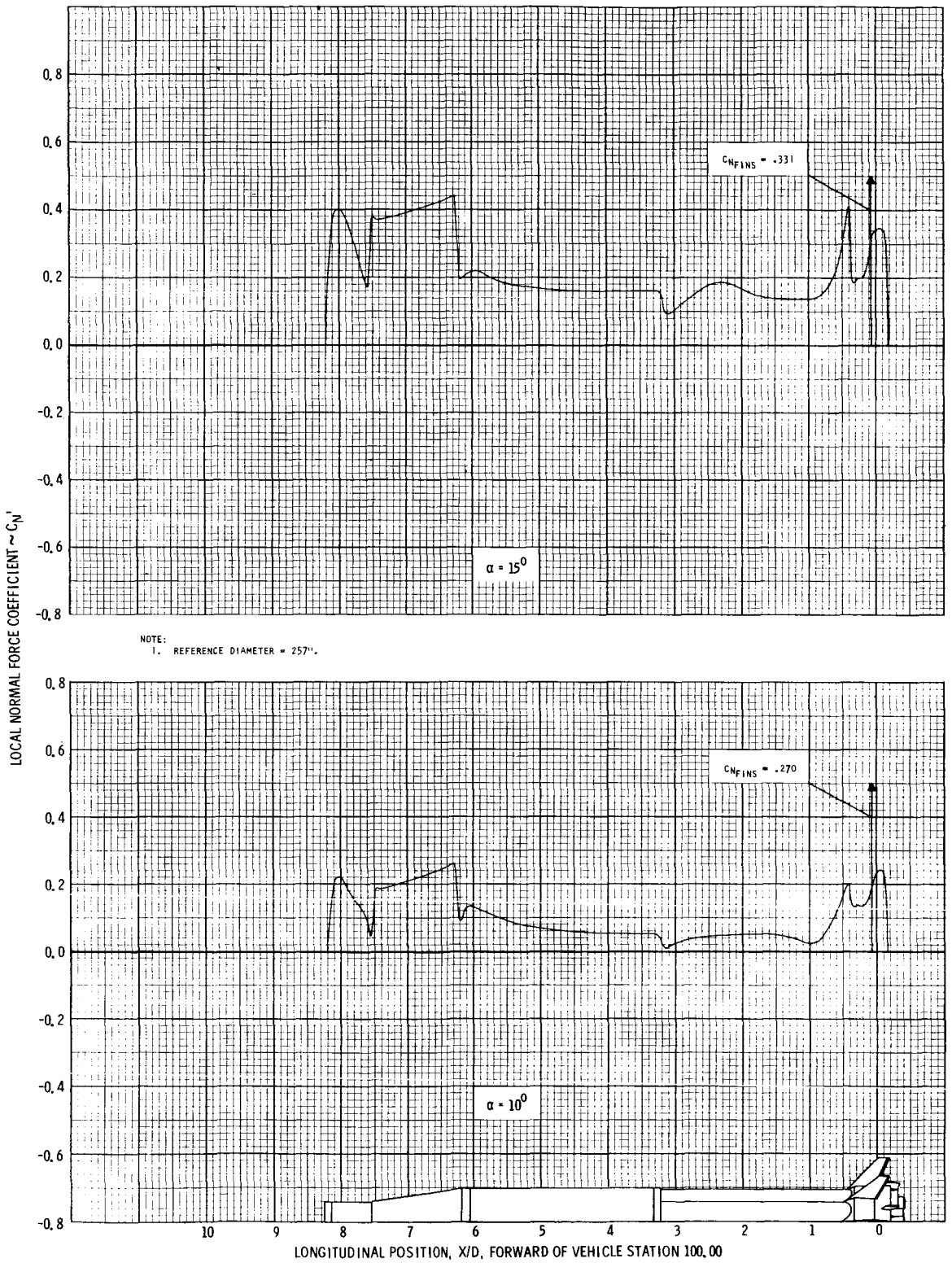

FIGURE 33: DISTRIBUTION OF LOCAL NORMAL FORCE COEFFICIENT AT MACH 2.16; α = 10° AND 15°.

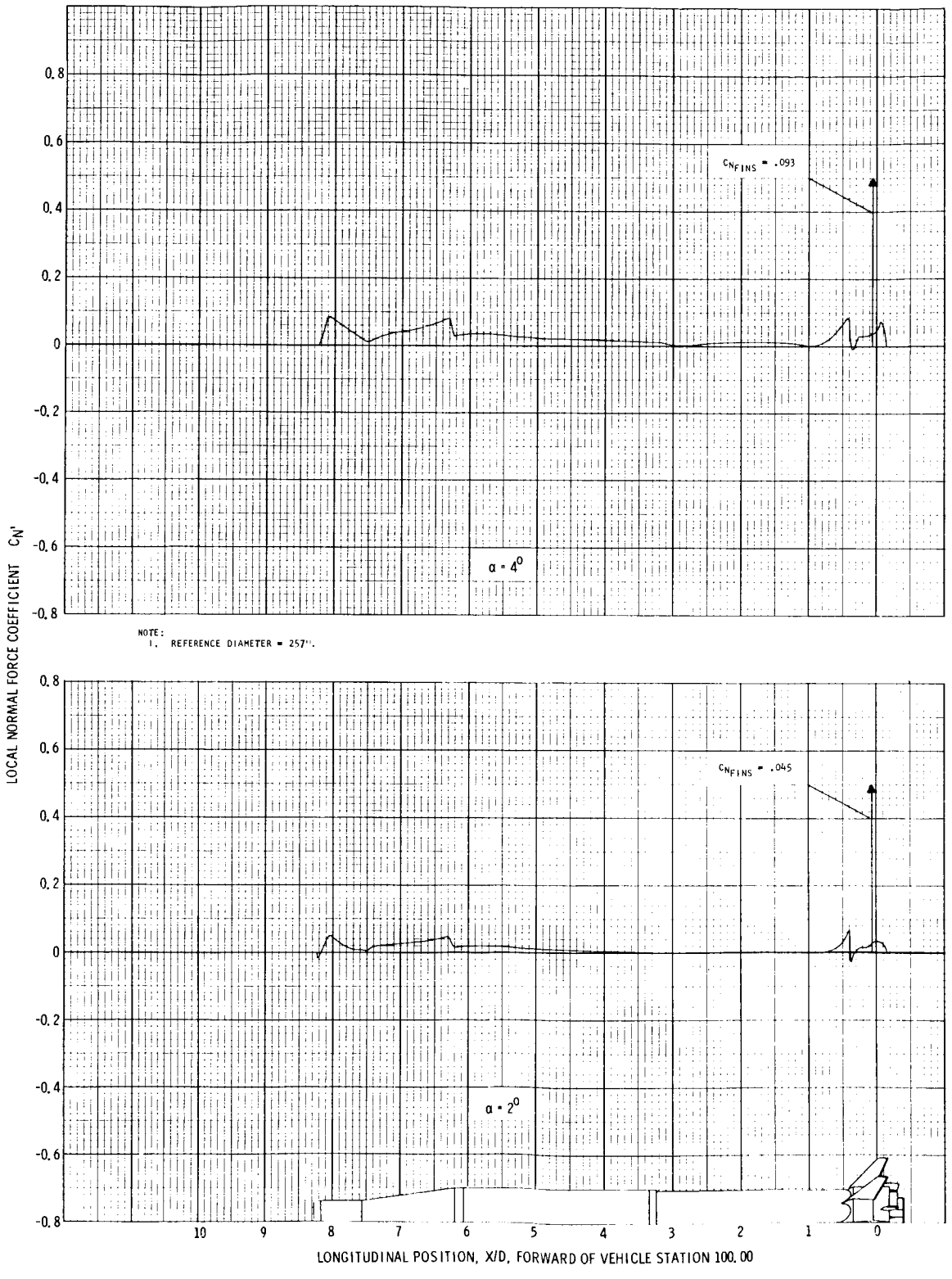

FIGURE 34: DISTRIBUTION OF LOCAL NORMAL FORCE COEFFICIENT AT MACH 2.86; $\alpha = 2^0$ AND 4^0.

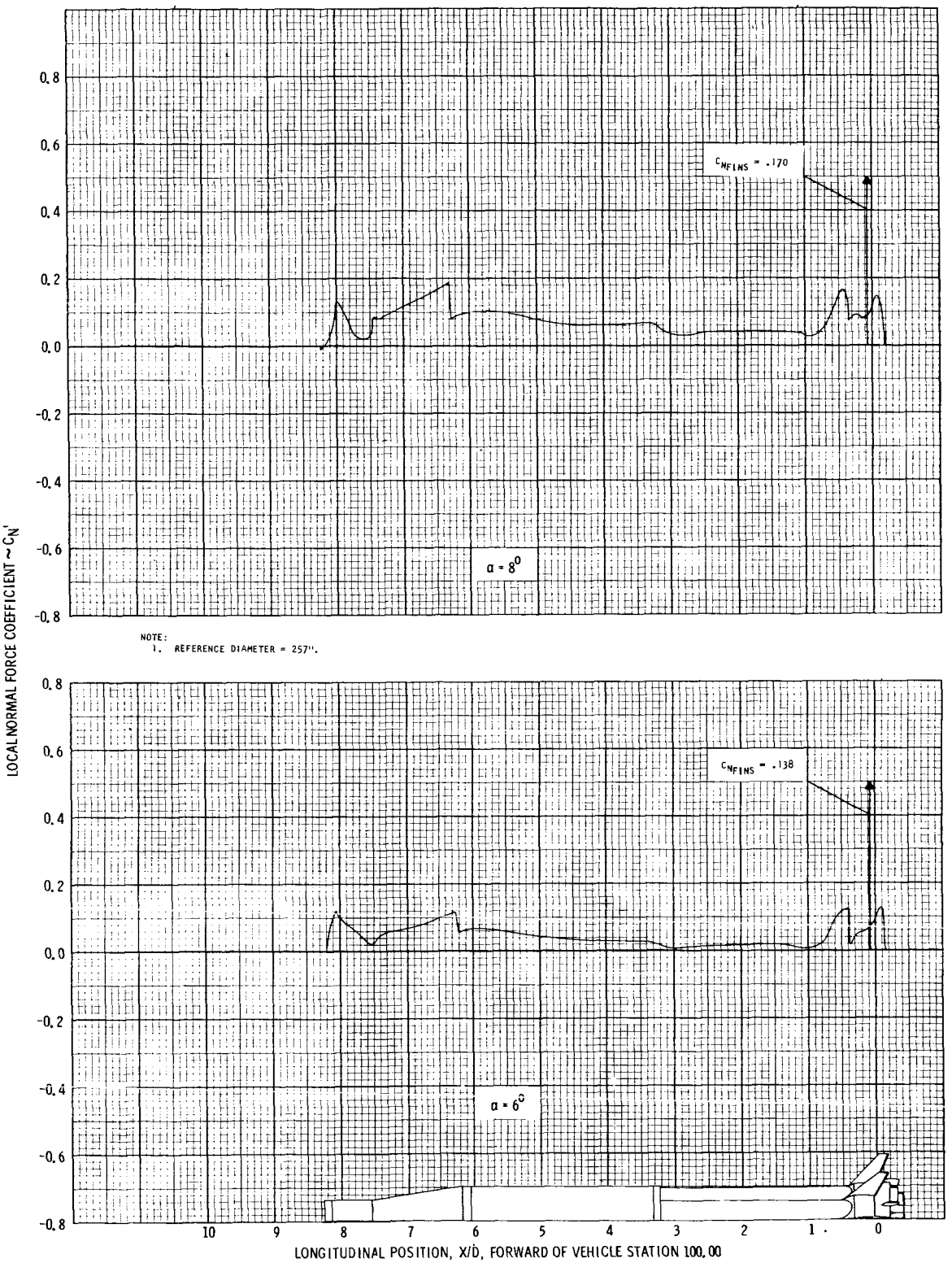

FIGURE 35: DISTRIBUTION OF LOCAL NORMAL FORCE COEFFICIENT AT MACH 2.86; α = 6° AND 8°.

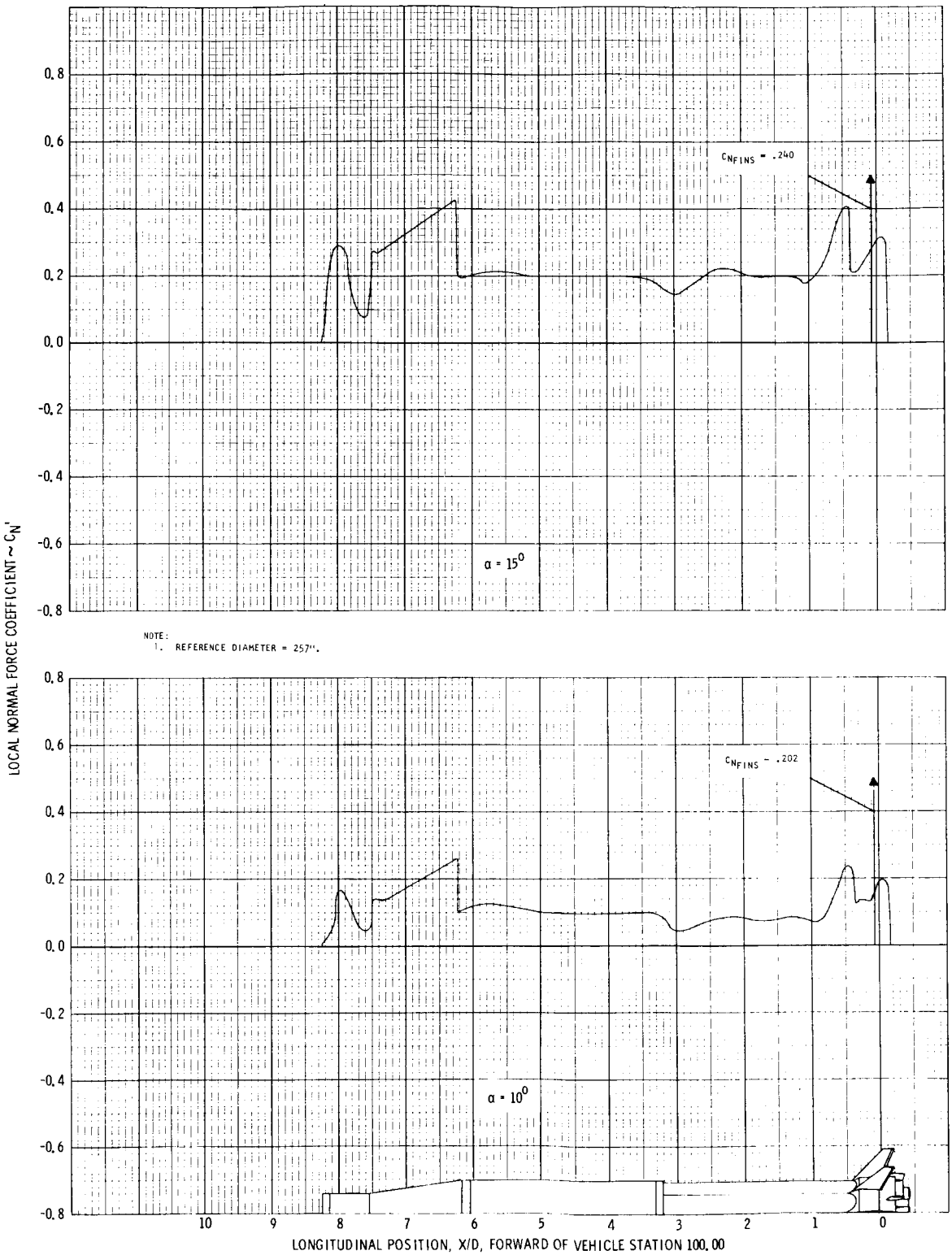

FIGURE 36: DISTRIBUTION OF LOCAL NORMAL FORCE COEFFICIENT AT MACH 2.86; $\alpha = 10^0$ AND 15^0.

C_A @ $\alpha = 0^0$ DUE TO VARIOUS COMPONENTS

MACH	SYMBOL	FRONT FACE f	b	SHROUDS	8 FINS*	BASE POWER OFF	BASE POWER ON	FRICTION PER CALIBER	VEHICLE
0.5	———	0.343	0.023	0.040	0.046	0.249	0.277	0.007	AS-201
0.8	- - - -	0.378	0.009	0.040	0.048	0.249	0.184	0.007	
0.9	—·—	0.394	0.005	0.040	0.065	0.261	0.186	0.007	
0.5	———	0.343	0.023	N/A	0.089	0.227	0.268	0.007	AS-202
0.8	- - - -	0.378	0.009	N/A	0.095	0.221	0.163	0.007	
0.9	—·—	0.394	0.005	N/A	0.106	0.235	0.166	0.007	
0.5	———	0.343	0.023	N/A	0.089	0.227	0.268	0.007	AS-204 AND SUBS.
0.8	- - - -	0.378	0.009	N/A	0.095	0.221	0.163	0.007	
0.9	—·—	0.394	0.005	N/A	0.106	0.235	0.166	0.007	

NOTES:
1. * DENOTES FRICTION DRAG IS INCLUDED IN TABULATED DATA.
2. ENGINE SKIRTS ARE REMOVED ON AS-202 AND ALL SUBSEQUENT VEHICLES.
3. TURBINE EXHAUST DUCT FAIRING ARE REMOVED ON AS-204 AND SUBSEQUENT VEHICLES. EXHAUST ROUTED INTO FLAME SHIELD AREA.

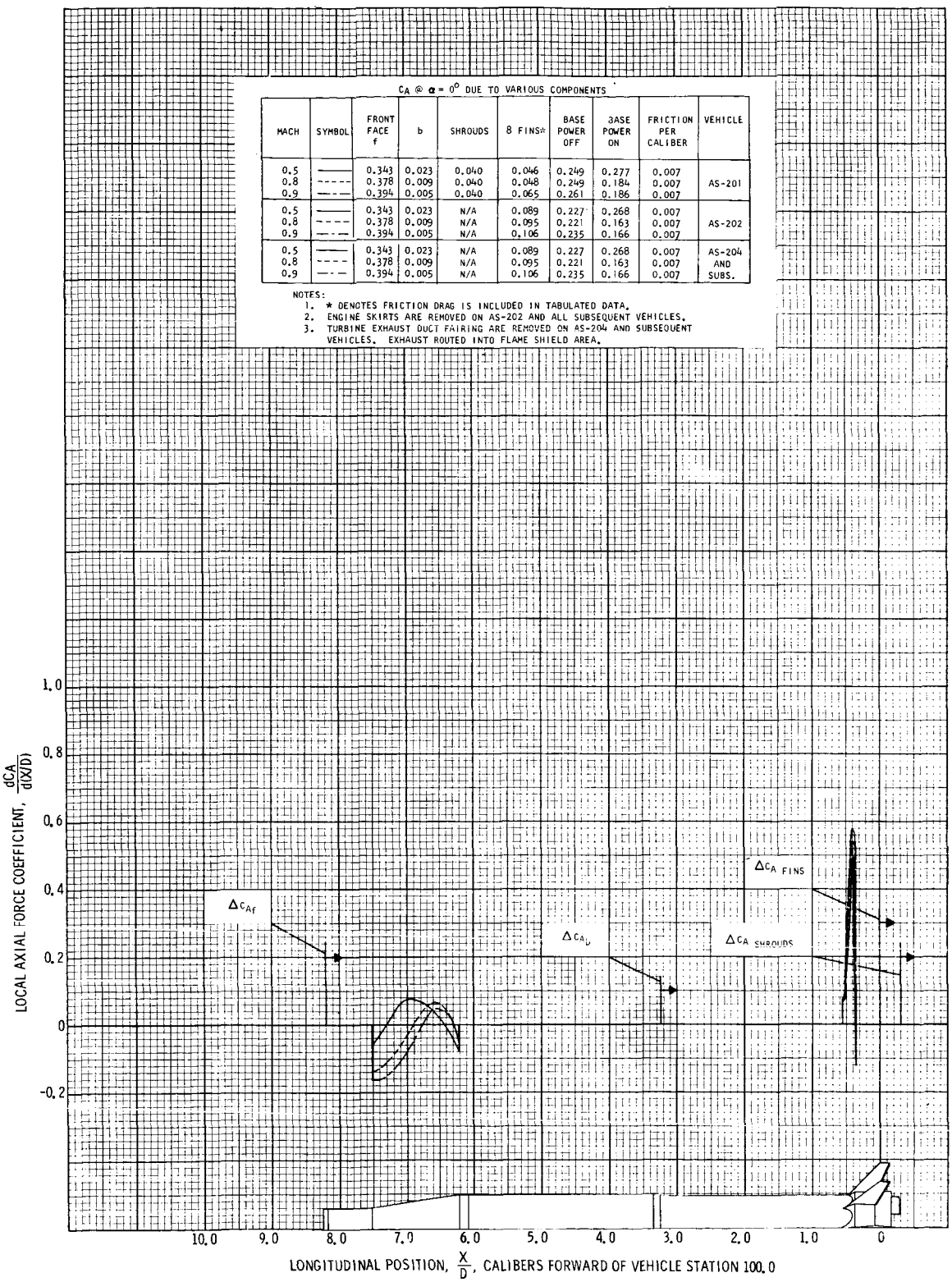

FIGURE 37 DISTRIBUTION OF LOCAL AXIAL FORCE COEFFICIENT AT $\alpha = 0^0$ FOR MACH 0.5, 0.8, AND 0.9

C_A @ $\alpha = 0^0$ DUE TO VARIOUS COMPONENTS

MACH	SYMBOL	FRONT FACE f	b	SHROUDS	8 FINS*	BASE POWER OFF	BASE POWER ON	FRICTION PER CALIBER	VEHICLE
1.0	——	0.410	0.008	0.045	0.092	0.322	0.275	0.007	AS-201
1.2	- - - -	0.446	0.047	0.062	0.087	0.431	0.148	0.006	
1.0	——	0.456	0.008	N/A	0.150	0.292	0.242	0.007	AS-202
1.2	- - - -	0.496	0.047	N/A	0.123	0.393	0.131	0.006	
1.0	——	0.456	0.008	N/A	0.150	0.292	0.242	0.007	AS-204 AND SUBS.
1.2	- - - -	0.496	0.047	N/A	0.123	0.393	0.126	0.006	

NOTES:
1. * DENOTES FRICTION DRAG IS INCLUDED IN TABULATED DATA.
2. ENGINE SKIRTS ARE REMOVED ON AS-202 AND ALL SUBSEQUENT VEHICLES.
3. TURBINE EXHAUST DUCT FAIRING ARE REMOVED ON AS-204 AND SUBSEQUENT VEHICLES. EXHAUST ROUTED INTO FLAME SHIELD AREA.

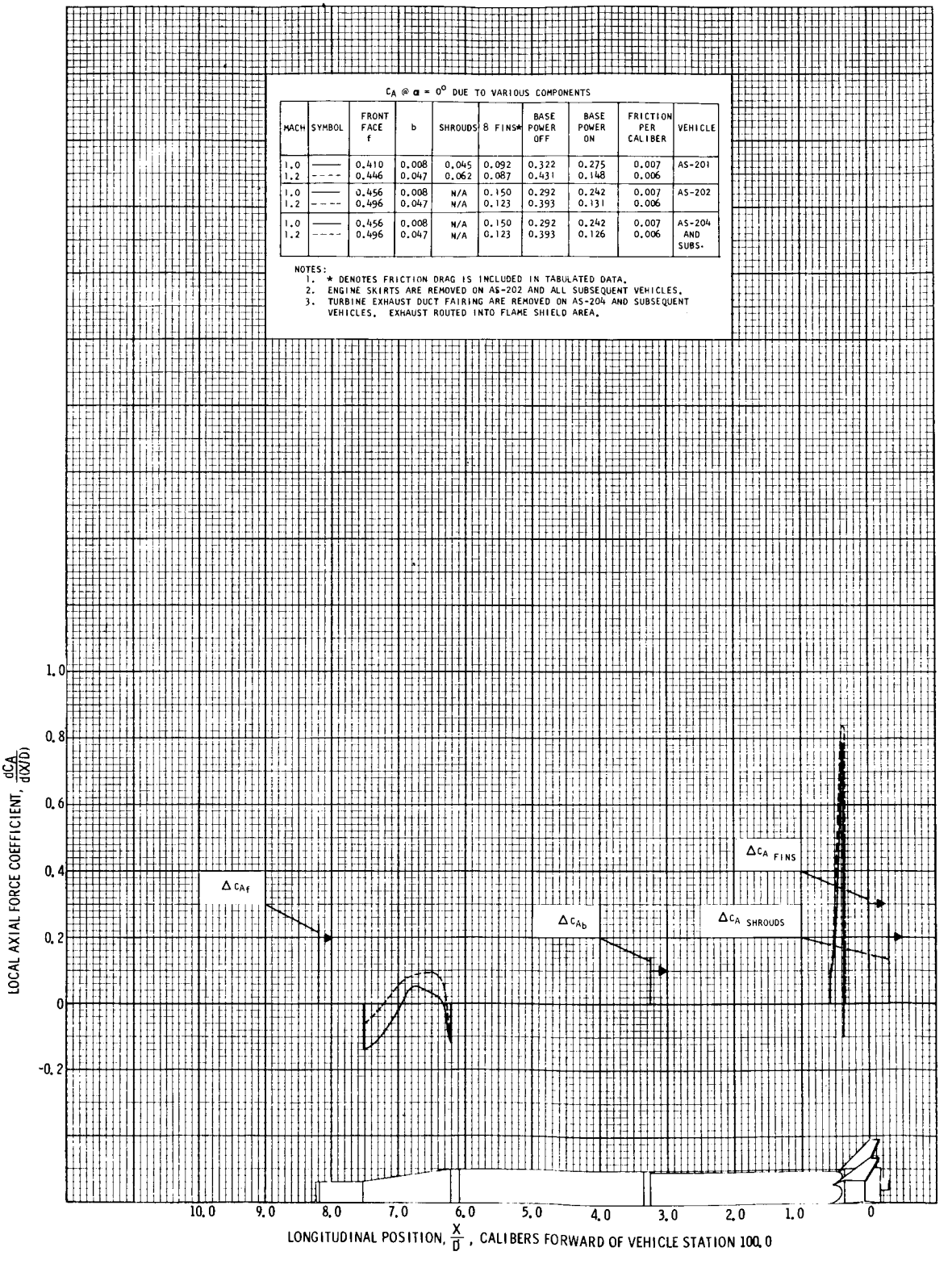

FIGURE 38 DISTRIBUTION OF LOCAL AXIAL FORCE COEFFICIENT AT $\alpha = 0^0$ FOR MACH 1.0 AND 1.2

C_A @ $\alpha = 0^\circ$ DUE TO VARIOUS COMPONENTS

MACH	SYMBOL	FRONT FACE f	b	SHROUDS	8 FINS*	BASE POWER OFF	BASE POWER ON	FRICTION PER CALIBER	VEHICLE
1.57	——	0.504	0.038	0.062	0.050	0.343	0.018	0.006	AS-201
2.16	- - - -	0.543	0.024	0.059	0.046	0.226	-0.099	0.006	
2.86	— - — -	0.564	0.012	0.041	0.042	0.133	-0.127	0.006	
1.97	——	0.504	0.038	N/A	0.085	0.311	0.014	0.006	AS-202
2.16	- - - -	0.543	0.024	N/A	0.060	0.210	-0.088	0.006	
2.86	— - — -	0.564	0.012	N/A	0.042	0.124	-0.113	0.006	
1.57	——	0.560	0.038	N/A	0.085	0.311	-0.002	0.006	AS-204 AND SUBS.
2.16	- - - -	0.603	0.024	N/A	0.060	0.210	-0.111	0.006	
2.86	— - — -	0.627	0.012	N/A	0.042	0.124	-0.171	0.006	

NOTES:
1. * DENOTES FRICTION DRAG IS INCLUDED IN TABULATED DATA.
2. ENGINE SKIRTS ARE REMOVED ON AS-202 AND ALL SUBSEQUENT VEHICLES.
3. TURBINE EXHAUST DUCT FAIRING ARE REMOVED ON AS-204 AND SUBSEQUENT VEHICLES. EXHAUST ROUTED INTO FLAME SHIELD AREA.

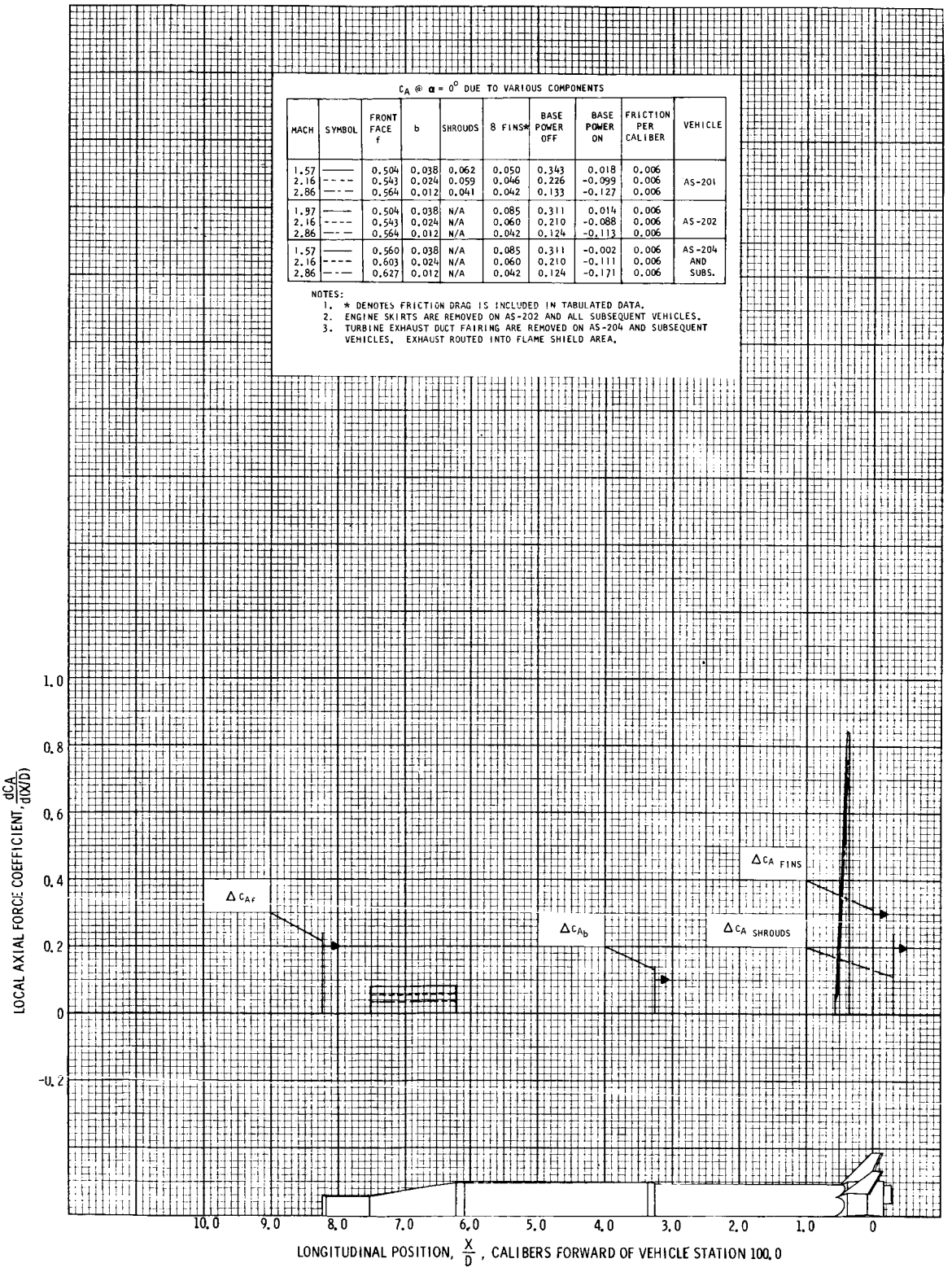

FIGURE 39 DISTRIBUTION OF LOCAL AXIAL FORCE COEFFICIENT AT $\alpha = 0^\circ$ FOR MACH 1.57, 2.16 AND 2.86

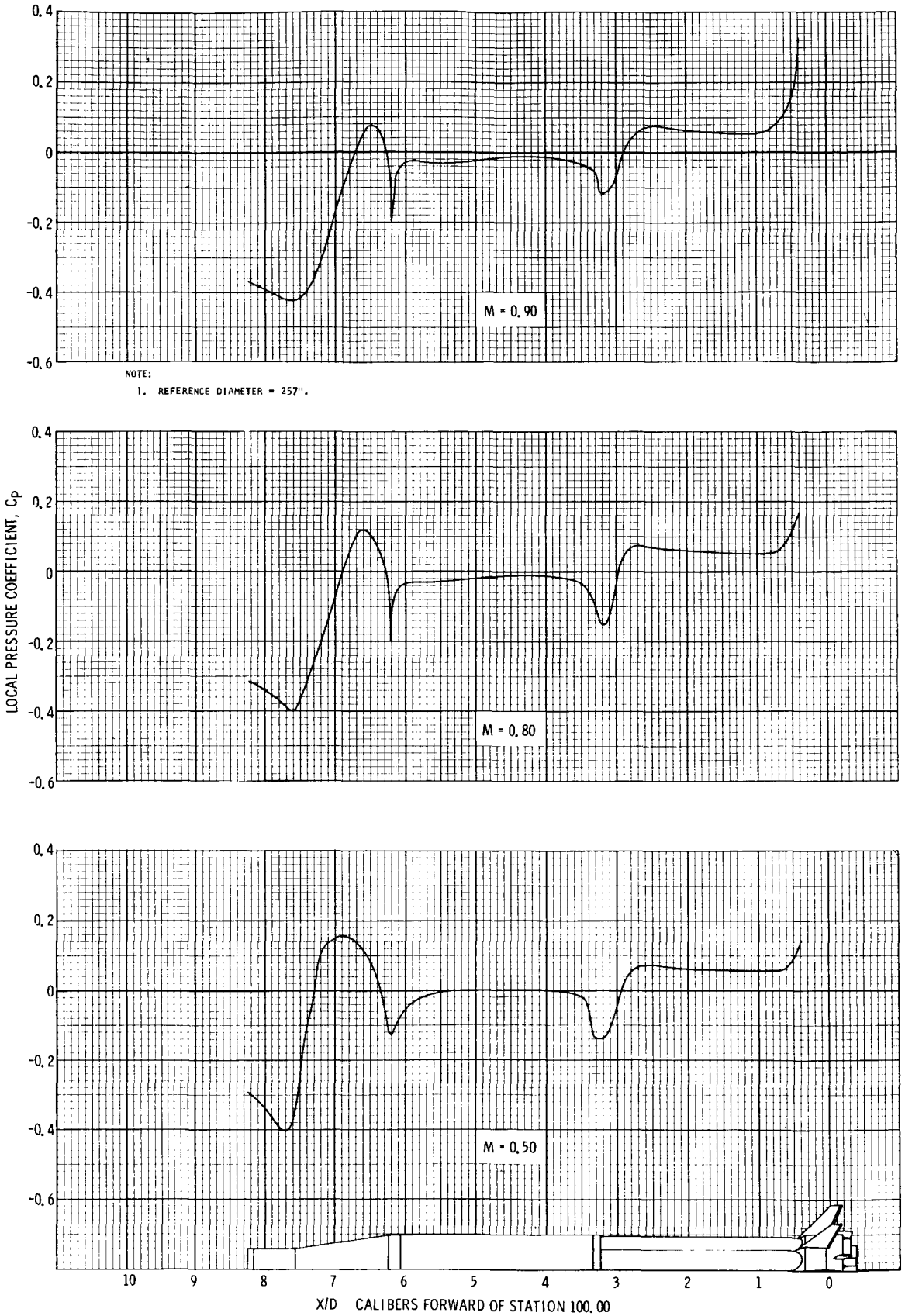

FIGURE 40: DISTRIBUTION OF LOCAL PRESSURE COEFFICIENT AT $\alpha = 0^0$ FOR MACH 0.5, 0.8, AND 0.9

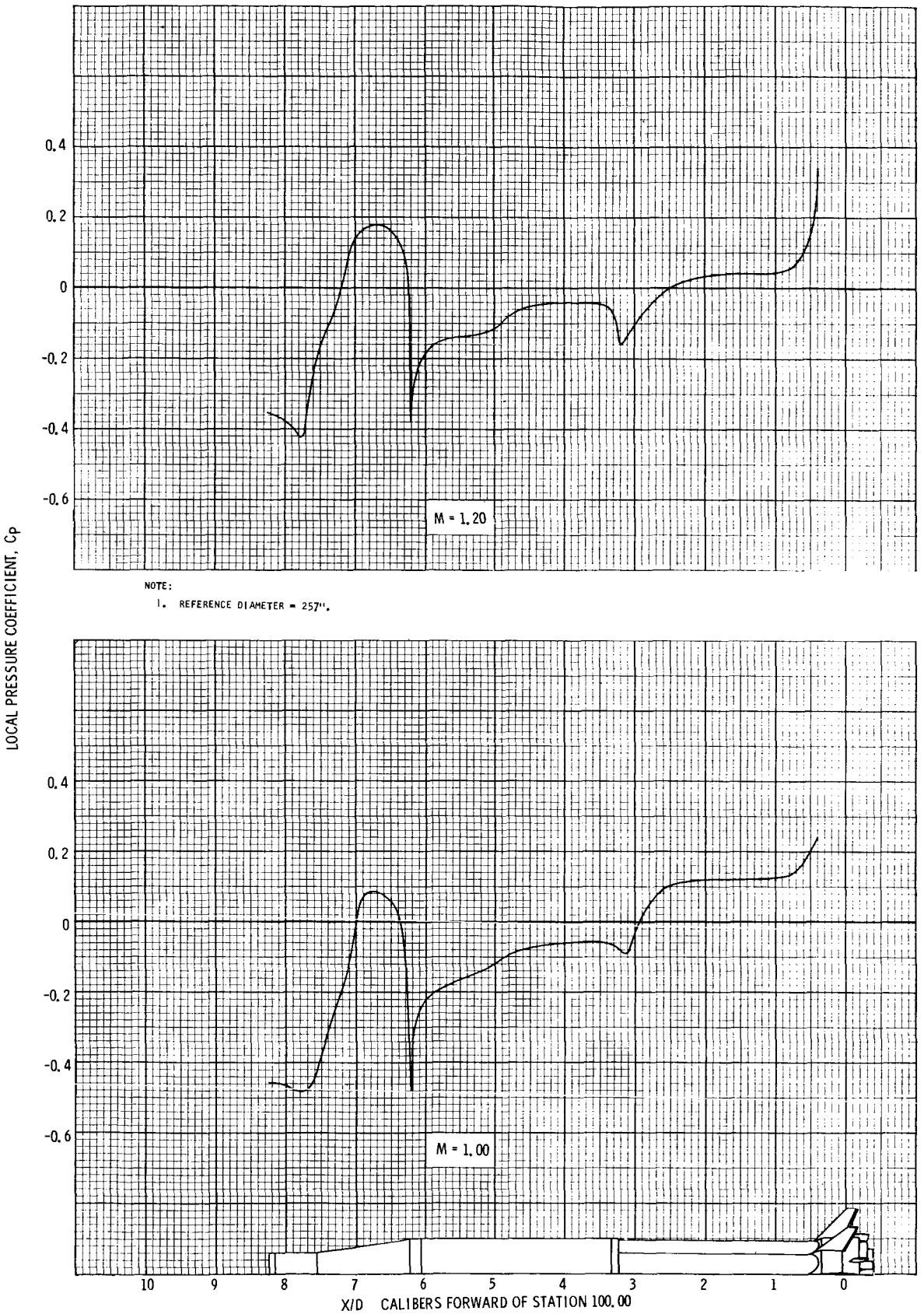

FIGURE 41: DISTRIBUTION OF LOCAL PRESSURE COEFFICIENT AT $\alpha = 0^0$ FOR MACH 1.0 AND 1.2

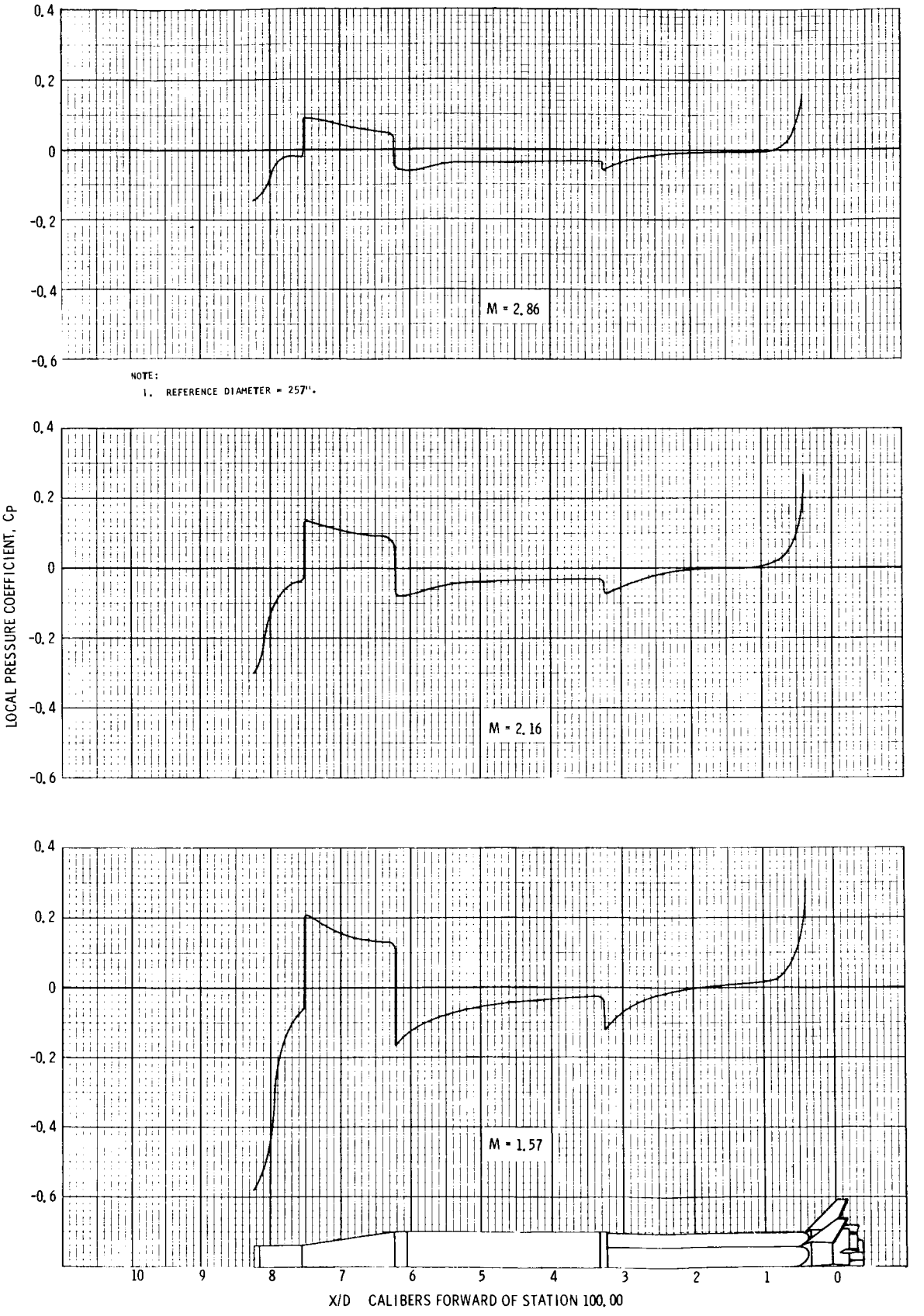

NOTE:
1. REFERENCE DIAMETER = 257".

FIGURE 42: DISTRIBUTION OF LOCAL PRESSURE COEFFICIENT AT $\alpha = 0^0$ FOR MACH 1.57, 2.16 AND 2.86

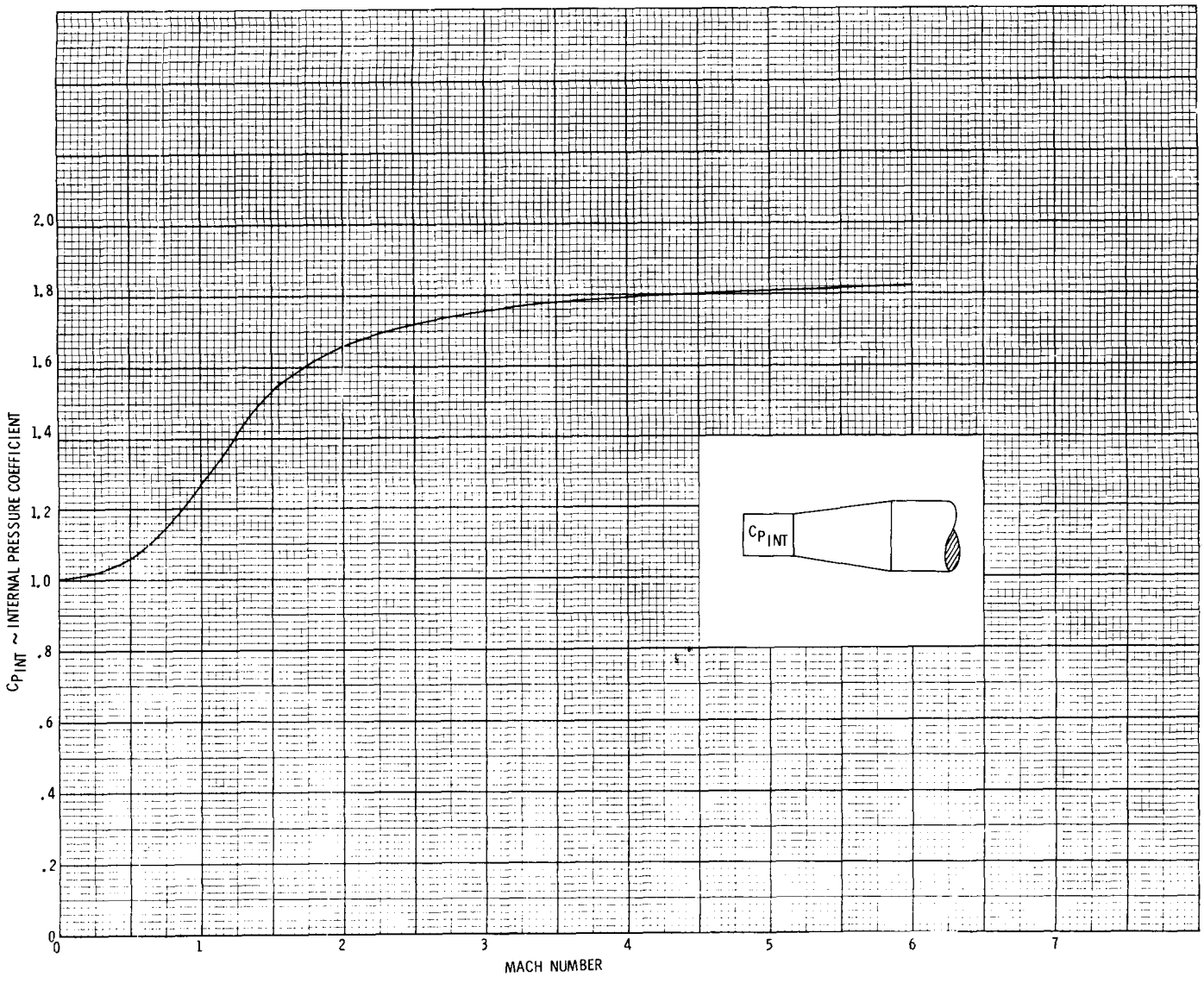

FIGURE 43 INTERNAL PRESSURE COEFFICIENT VERSUS MACH NUMBER

REFERENCES

1. Ashman, G. F., "Saturn IB/Apollo Aborted Configuration Aerodynamic Characteristics," CCSD-TB-AE-65-145, March 5, 1965, Unclassified.

2. Pitcock, R. E., "Experimental Static Longitudinal Stability and Drag Characteristics of the Saturn IB/Apollo Vehicle," R-AERO-AD-108-63, October 7, 1963, Unclassified.

3. Johnson, J. D., "Experimental Static Longitudinal Stability and Drag Characteristics of a 1.32 Percent Scale Model of the Saturn IB/Apollo Vehicle in the Chance-Vought Corporation High Speed Wind Tunnel (M = 0.6 to 4.75)," R-AERO-AD-64-26, March 4, 1964, Unclassified.

4. Johnson, J. D., "Static Longitudinal Stability and Axial Force Characteristics of the Saturn IB/Apollo Launch Vehicle as Determined from Tests of a 1.32 Percent Scale Model at Langley Research Center," R-AERO-AD-64-94, October 15, 1964, Unclassified.

5. Reese, H. B., "Results of a Wind Tunnel Investigation to Determine the Pressure and Local Normal Force Distribution over the Saturn IB Vehicle," CCSD-TN-AE-63-3, August 1, 1963, Unclassified.

6. Chianese, F., "Static Pressure and Normal Force Coefficient Distributions on the Saturn IB Launch and Aborted Launch Configuration as Determined from Wind Tunnel Tests," CCSD-TN-AE-64-12, December 30, 1963, Unclassified.

7. Cornell Aeronautical Laboratory, Inc., "Transonic Wind Tunnel Test of a 0.0175 Scale Pressure Model of the Saturn C-1, Block II Configuration," CAL-HM-1510-Y-8, July 1, 1963, Unclassified.

8. Nunley, B. W., "Static Aerodynamic Characteristics of the Apollo-Saturn IB Vehicle," NASA TM X-53348, October 13, 1965, Unclassified.

9. Romberg, Gary F., "Results of a Wind Tunnel Investigation to Determine the Detailed Pressure Distribution on the S-IB Stage Fin and Tail Area of the Saturn IB Vehicle," CCSD-TN-AE-65-72, February 15, 1965, Unclassified.

STATIC AERODYNAMIC CHARACTERISTICS OF THE ABORTED APOLLO-SATURN IB VEHICLE

By

Billy W. Nunley

The information in this report has been reviewed for security classification. Review of any information concerning Department of Defense or Atomic Energy Commission programs has been made by the MSFC Security Classification Officer. This report, in its entirety, has been determined to be unclassified.

This document has also been reviewed and approved for technical accuracy.

Bob G. Dunn
Chief, Vehicle Aerodynamics Section

for Ellery B. May
Chief, Aerodynamic Design Branch

Werner K. Dahm
Chief, Aerodynamics Division

E. D. Geissler
Director, Aero-Astrodynamics Laboratory

DISTRIBUTION

DIR
Dr. von Braun

MS-IPL (8)

MS-IP

MS-H

HME-P

CC-P

MS-T (6)

R-ASTR
Mr. Moore
Mr. Hosenthien
Mr. Blackstone
Mr. Brandner
Mr. Richard

R-P&VE
Dr. Lucas
Mr. Palaoro
Mr. Aberg
Mr. Glover
Mr. Kamback
Mr. Goerner
Mr. Blumrich
Mr. Furman
Mr. Showers (3)
Mr. Verble

R-AS
Mr. Spears

R-AERO
Dr. Geissler
Mr. Jean
Mr. Ryan
Mr. Lovingood
Mr. Lindberg
Mr. Hagood
Mr. Stone
Mr. McNair (6)
Mr. Teague (7)
Mr. Dahm
Mr. Reed
Mr. Wilson

R-AERO
Mr. May
Mr. Andrews
Mr. Dunn
Mr. Nunley

EXTERNAL

Scientific and Technical Information
Facility (25)
Attn: NASA Representative (S-AK/RKT)
P. O. Box 5700
Bethesda, Maryland

Mr. John O. Windham
MSFC Resident Liaison Engineer
NASA, Langley Research Center
Langley Station, Building 1218
Hampton, Virginia 23365

Mr. E. A. Rawls
Chrysler Corporation Space Division
Michoud Operations
Aerodynamics Group
P. O. Box 29200
New Orleans, Louisiana 70129

Mr. C. H. Perrine
NASA, Manned Spacecraft Center
Apollo Spacecraft Program Office
Systems Engineering Division
618 Building 2, Code PS3
Houston, Texas 77058